Transportation Research Part C 190 (2026) 105790

Contents lists available at ScienceDirect

Transportation Research Part C

journal homepage: www.elsevier.com/locate/trc

A multi-objective approach for coordinating railway transport and electric demand-oriented services considering opportunity charging

Androniki Dimitriadou [a,*], Konstantinos Gkiotsalitis [a], Tao Liu [b], Oded Cats [c]

[a] National Technical University of Athens, School of Civil Engineering, Department of Transportation Planning and Engineering, Zografou Campus, 9, Iroon Polytechniou str, Athens, 15773, Greece
[b] National Engineering Laboratory of Integrated Transportation Big Data Application Technology, National United Engineering Laboratory of Integrated and Intelligent Transportation, School of Transportation and Logistics, Southwest Jiaotong University, Chengdu, 611756, China
[c] Delft University of Technology, Faculty of Civil Engineering and Geosciences, Building 23, Stevinweg 1, Delft, 2628 CN, The Netherlands

ARTICLE INFO

Keywords:
Electric demand-oriented services
Multi-objective optimization
Opportunistic charging
Public transport rescheduling
Travel-time uncertainty
Vehicle routing problem

ABSTRACT

Electrification is reshaping Mobility-on-Demand (MoD), yet coordinating electric demand-oriented shuttles with public transport remains challenging due to the interaction of routing, charging, and timetable decisions. This study introduces an Electric Vehicle Routing and Public Transport Rescheduling model (EVRP–PTR) that jointly assigns electric shuttle feeder services to passenger requests, schedules opportunity charging through in-network pantographs while maintaining time continuity in the charging process, and reschedules public transport departures to improve transfer synchronization. The problem is bi-objective, minimizing passenger door-to-public transport travel time and shuttle operating costs while accounting for travel-time uncertainty. Initially formulated as a mixed-integer nonlinear program (MINLP), the model is reformulated as a mixed-integer linear program (MILP), enabling the computation of globally optimal solutions. Due to the multi-objective nature of the problem, the Pareto front is obtained using the ϵ-constraint method. A case study in Athens, Greece, where electric shuttles feed the Athens–Thessaloniki railway corridor with five pantograph locations, shows that modest fleet increases substantially reduce passenger travel times and eliminate the need for en-route charging in some Pareto-optimal solutions. Under travel-time uncertainty, service-performance gains become less pronounced, and larger on-demand fleets are required to maintain comparable service quality. The proposed framework remains computationally tractable for mid-sized networks and can support tactical planning and opportunity-charging scheduling by quantifying trade-offs between service quality and fleet resources in integrated PT–EMoD systems.

1. Introduction

Global urban transport is undergoing rapid transformation driven by electrification and multi-modal integration (Harris et al., 2015; McCoy et al., 2018; Makarova et al., 2023; Aidam et al., 2025). In countries such as the Netherlands and Singapore, integrated mobility systems already combine rail and public transport with bicycle-sharing and car-sharing services to improve

* Corresponding author.
E-mail address: adimitriadou@mail.ntua.gr (A. Dimitriadou).

https://doi.org/10.1016/j.trc.2026.105790
Received 17 October 2025; Received in revised form 28 May 2026; Accepted 29 May 2026
Available online 5 June 2026

first/last-mile connectivity (Greenwheels, 2026; HelloRide Singapore, 2026; , NS; SBS Transit, 2026). In Singapore, these initiatives are further aligned with the Land Transport Master Plan 2040, which promotes integrated and sustainable multi-modal mobility systems (Land Transport Authority Singapore, 2019). These developments increasingly extend to Mobility-on-Demand (MoD) systems, where Shared Electric Vehicles (SEVs) complement public transport by dynamically serving ride requests and recharging when required, contributing to lower emissions, reduced congestion, and improved accessibility (Wang and Guo, 2022).

Demand-responsive transport (DRT) provides a flexible, user-oriented complement to fixed-route public transport, which often struggles to accommodate heterogeneous and time-varying demand (Alonso-González et al., 2017; Zhang and Wu, 2023). Efficient integration between on-demand mobility and public transport (PT) requires operational coordination, particularly in feeder-trunk systems where feeder arrivals should align with trunk-service departures to minimize transfer times (Ceder, 2016; Liu et al., 2021; Gkiotsalitis et al., 2023). Research on MoD–PT integration spans both behavioral and operational perspectives, including studies on user acceptance and willingness to pay, as well as analytical frameworks for pricing, service design, and routing optimization (Salazar et al., 2018; Steiner and Irnich, 2020; Xiong et al., 2020; Dimitriadou and Gkiotsalitis, 2025; Liyanage and Dia, 2025).

Advances in communication and positioning technologies (i.e., GPS-enabled smartphones) have transformed DRT from traditional dial-a-ride systems into app-based, flexible mobility services, as demonstrated by deployments such as BerlKönig in Berlin, XBUS in Lisbon, Zeelo in the UK, and services offered by Uber and Cabify (ViaVan, 2018; State of Berlin, 2022; ITS International, 2022; Shotl, 2022; Cabify, 2025; Uber Technologies, 2025; Zeelo, 2025). At the same time, transport remains a major contributor to CO_2 emissions and urban NO_x pollution in European cities, increasing the need for decarbonized public mobility (International Energy Agency, 2023; European Environment Agency, 2024). Evidence suggests that well-designed on-demand ridesharing can reduce congestion and emissions, particularly when electrified, whereas poorly integrated services may increase dependence on private vehicles, highlighting the importance of strong PT integration (Kaddoura et al., 2020; Dang et al., 2021; Melo et al., 2024).

Implementing electric DRT (e-DRT) requires accounting for real-world operational variability, including travel-time uncertainty, charging logistics, station capacities, and state-of-charge (SOC) constraints (Ahani et al., 2023). Motivated by these challenges, this study considers opportunity (en-route) pantograph charging, enabling fast intermediate top-ups to improve vehicle availability.

Throughout this study, we develop a tactical modeling framework for the coordinated integration of electric demand-oriented (on-demand) shuttle buses (feeder service) with the railway system (primary trunk mode). Coordination is achieved through the joint optimization of shuttle routing, opportunity charging, and railway timetable adjustments. Passenger demand is assumed to be known in advance over the planning horizon; therefore, *on-demand service* refers to a flexible, non-fixed route transport service responding to passenger requests for trips to the railway station. In addition, *door-to-rail travel time* is defined as the total passenger travel time from pickup request until boarding the time-appropriate railway service.

The main contributions of this study are summarized as follows:

a. Developed a unified three-layer EVRP–PTR framework integrating the Electric Vehicle Routing Problem (EVRP), opportunity charging scheduling, and Public Transport Rescheduling (PTR).
b. Formulated the EVRP–PTR as a mixed-integer nonlinear program (MINLP) and reformulated it as a mixed-integer linear program (MILP).
c. Modeled opportunistic (re)charging at publicly accessible charging stations without predefined time slots.
d. Incorporated travel-time uncertainty to better capture real-world operational variability in on-demand services.
e. Evaluated the EVRP–PTR framework through an Athens case study and complementary analyses, demonstrating the impact of PT timetable flexibility on system performance and the applicability of the model to multi-origin shuttle operations.

The EVRP–PTR is formulated as a multi-objective optimization problem (MOOP) with two conflicting objectives that aim to minimize: (i) the required number of electric on-demand shuttles and (ii) total door-to-rail passenger travel time. The ϵ-constraint method is employed to generate non-dominated Pareto-optimal solutions, illustrating the trade-offs between service quality and fleet utilization. The resulting framework can support tactical decision-making for integrated PT–EMoD planning.

The remainder of the paper is structured as follows. Section 2 reviews related work on electric mobility-on-demand (EMoD) services and their integration with public transport (PT). Section 3 presents the mathematical formulation of the EVRP–PTR and its mixed-integer linear program (MILP) reformulation. Section 4 extends the model formulation to incorporate travel-time uncertainty in on-demand operations. Section 5 presents experiments on a toy network with synthetic data and a real-world case study in Athens, Greece, together with additional analyses, including computational performance evaluation, sensitivity analysis of the Public Transport Rescheduling (PTR) model, travel-time uncertainty assessment, and a multi-origin shuttle scenario evaluating the applicability of the EVRP–PTR framework to networks with multiple shuttle origin points (depots). Finally, the paper concludes with key findings and future research directions.

2. Literature review

This section is organized around two subsections. First, it reviews the Electric Mobility-on-Demand (EMoD) literature, synthesizing research goals, methodological approaches (i.e., optimization, simulation, learning-based control), and operational strategies. Second, it reviews studies that integrate EMoD with public transport (PT). Finally, key knowledge gaps are identified, outlining how this study advances the state of the art.

2.1. Electric mobility-on-demand services

Simulation software has been used in the past for electric MoD services. Doubleday et al. (2016) introduced WPTSim, a high-resolution simulation tool (one-second speed/location/road grade data) to explore how wireless power transfer (WPT) could be integrated into an on-demand shuttle operation, showing that even a single in-route WPT site can dramatically shrink the required battery capacity (in some scenarios by more than half). Liang et al. (2021) then modeled the joint decision-making of a shared on-demand electric vehicle (EV) fleet—charging scheduling, order dispatching, and rebalancing—as a (partially observable) Markov Decision Process (MDP), solved with deep reinforcement learning coupled to a binary linear assignment at each step. The trained network estimated mobility-aware state values over time, location, and state-of-charge (SOC), enabling vehicles to schedule top-ups and dispatches. Simulations showed that the learned policy stabilizes charging patterns and outperforms baseline rules. Complementing these, Li et al. (2022) developed a joint routing-charging model for e-DRT with opportunity charging during layovers. Solving it with a customized Variable Neighborhood Search (VNS) demonstrated an improvement of $\sim 11\%$ to the total-cost reduction relative to a full-charge baseline.

Surveying the broader field, Tan et al. (2022) provided a systematic review of scheduling and charging for shared MoD with electric fleets, classifying strategies, comparing modeling approaches (mathematical programming, reinforcement learning, hybrids), and mapping open problems. Esteban et al. (2025) analyzed a data-driven case study of a neighborhood on-demand transit (ODT) pilot in downtown St. Louis with low-speed electric vehicles (LSEVs). The authors used surveys, ridership logs, and vehicle trajectories, finding shorter trips than those of fixed route transit.

Recent studies have focused on shared autonomous electric vehicles (SAEVs). Jäger et al. (2017) evaluated a shared, autonomous, electric on-demand concept in Munich, showing the strongest environmental gains under ride-pooling and renewable electricity. Tucker et al. (2019) proposed an online primal-dual welfare-maximization algorithm for real-time charge scheduling and rebalancing under charger-capacity limits for autonomous mobility-on-demand services (AMoD). Badia and Jenelius (2021) used a continuum-approximation model to compare fixed-route against door-to-door demand-responsive feeders to trunk transit, finding automation to be the dominant driver of feeder choice, with electrification effects being comparatively modest.

Continuing within the electric AMoD field, Wang and Guo (2022) focused on dynamic dispatching of SAEVs in Mobility-on-Demand (MoD) systems. They assigned vehicles to three concurrent tasks: recharging, serving trips, and repositioning. The authors modeled the fleet's operations as a multi-agent, multi-task problem within a Markov Decision Process (MDP) framework, and integrated combinatorial optimization with deep reinforcement learning. Addressing the core charging problem of AMoD, Gao and Li (2024) compared plug-in charging with battery swapping via a bi-level mathematical program with equilibrium constraints (MPEC) solved as a mixed-integer nonlinear programming model (MINLP) with queuing-based congestion and elastic demand. A complementary line of studies couples AMoD with the power system: an optimal power flow (OPF)-coupled formulation showed that coordinated charging can eliminate $\sim 99\%$ of feeder overloads and $\sim 50\%$ of voltage drops (Estandia et al., 2021). Additionally, earlier linear flow models of AMoD demonstrated significant energy-cost savings under joint coordination (Rossi et al., 2019).

Considering past studies at the operational level, early agent-based studies established how battery range and charger time/placement shape SAEV fleet size, service quality, and emissions (Chen et al., 2016). Pricing works showed that dynamic fares for SAEVs can cut waiting times by $\sim 19-23\%$ while trading off revenue and equity (Chen and Kockelman, 2016). The US National Renewable Energy Laboratory (NREL) summarized the operational challenges of automated electric on-demand fleets (i.e., charge planning during service) and mapped opportunities for algorithmic and infrastructural advances (Lott and Young, 2023). On joint design-operation, Paparella et al. (2024) formulated a mixed-integer linear program (MILP) that co-optimizes vehicle design (battery size, fleet size) and fleet operations to maximize operator profit. This study was extended to ride-pooling electric AMoD (E-AMoD) with charging-infrastructure modeled as a multilayer network-flow MILP (Paparella et al., 2025). Operationally, Boewing et al. (2020) developed a MILP for vehicle coordination and charging scheduling, balancing dispatch and (dis)charging under SOC and charger capacity limits. Finally, regional joint planning-operations have shown the value of integrating fleet, charging schedules, and dispatching (Sheppard et al., 2019).

Overall, the EMoD literature to date has mainly focused on electric fleet deployment, with charging emerging as a central design consideration. Existing studies mainly examine wireless/opportunity charging, charging scheduling, and joint routing–charging decisions. However, only a limited number of studies co-optimize fleet size and charging planning to balance cost, service quality, and the operational feasibility of on-demand services.

2.2. Electric on-demand services integrated with public transport systems

Turning to EMoD and public transport integration, Hsueh et al. (2021) used BEAM (a mesoscopic, agent-based extension of MATSim calibrated for the nine-country San Francisco Bay Area) to simulate countywide deployment of on-demand automated electric shuttles as first-/last-mile feeders to frequent transit in Santa Clara County, testing geofenced service areas and sensitivities (catchment radius, pricing, simulation horizon, initial vehicle placement, vehicle size, maximum speed) and reporting mode-share and energy impacts. Building an optimization counterpart, Fang and Ma (2023) proposed an on-demand first-mile electric feeder service synchronized with a public transport line, formulating a MILP that co-decides meeting-point pickups, arrival-time synchronization to specific train/bus departures, and capacitated partial recharging. At a broader systems level, Fang (2025) introduced the concept of electric integrated demand-responsive transport (e-DRT) which refers to an EV-based DRT explicitly synchronized with fixed-route mass transit. They also developed models and algorithms for fleet sizing, charger sizing, and schedule coordination under stochastic demand, with the policy aim of shifting trips to public transport.

Table 1
Literature summary. AMoD: Autonomous Mobility-on-Demand, DRL: Deep Reinforcement Learning, MILP: Mixed-Integer Linear Problem, MoD: Mobility-on-Demand, MPEC: Mathematical Program with Equilibrium Constraints, PT: Public Transport, VNS: Variable Neighborhood Search, WPT: Wireless Power Transfer.

Reference	Fully Electric MoD	PT Integration	Charging Location	Charging Type	Charger Scheduling	Passenger Waiting	MoD Fleet Size	Solution Method
(Doubleday et al., 2016)	✓		In-route WPT	Partial				WPTSim tool
(Jäger et al., 2017)	✓ (AMoD)							Simulation
(Tucker et al., 2019)	✓ (AMoD)		In-service plug-in points	Partial	✓			Heuristic
(Hsueh et al., 2021)	✓ (AMoD)	✓						Simulation
(Liang et al., 2021)	✓		In-service plug-in points	Full				DRL
(Li et al., 2022)	✓		In-service opportunity points	Partial	✓			Heuristic (VNS)
(Tan et al., 2022)	✓							Systematic review
(Wang and Guo, 2022)	✓ (AMoD)						✓	DRL
(Fang and Ma, 2023)	✓	✓	Private plug-in chargers	Partial	✓	✓		MILP
(Gao and Li, 2024)	✓ (AMoD)		Plug in or swap out	Full/partial			✓	Bi-level MPEC
(Paparella et al., 2024)	✓ (AMoD)		Plug-in charging stations	Partial	✓			MILP
(Esteban et al., 2025)	✓							Community survey
(Fang, 2025)	✓	✓	Plug-in charging stations	Partial	✓	✓		MILP
This study	✓	✓	Public opportunity chargers	Partial	✓	✓	✓	MILP

Although studies jointly addressing EMoD–PT integration and explicit charging operations remain limited, they are closely aligned with the present research. Building on this line of work, the proposed study jointly optimizes EMoD–PT coordination, electric fleet charging schedules, and fixed-line public transport timetable rescheduling to achieve tighter system-level integration.

2.3. Study contribution

The most relevant studies in past literature are summarized in Table 1. In summary, most studies focus on Electric Mobility-on-Demand (EMoD) in general, while far fewer examine the integration of EMoD with public transport.

In light of prior work, our problem coordinates electric on-demand services with fixed public transport while explicitly incorporating vehicle charging. As shown in Table 1, most EMoD studies rely on heuristic/metaheuristic approaches, whereas exact EMoD–PT formulations do not jointly optimize passenger travel times and operating costs. The integrated EVRP–PTR framework proposed in this study is formulated as a bi-objective optimization problem minimizing total door-to-rail passenger travel time and on-demand operating costs. The problem is solved using an exact solution approach based on the ϵ-constraint method, enabling the computation of globally optimal solutions and the generation of Pareto-optimal trade-offs. The following sections present the EVRP–PTR formulation, together with its implementation on a toy network and an extended real-world Athens case study, followed by the corresponding results analysis.

3. Formulation as an electric vehicle routing and public transport tescheduling problem

3.1. Problem description

The Electric Vehicle Routing and Public Transport Rescheduling Problem (EVRP–PTR) extends the Vehicle Routing and Public Transport Rescheduling Problem (VRP–PTR) (Dimitriadou and Gkiotsalitis, 2025) by incorporating a fleet of electric vehicles for on-demand mobility services. Similar to the VRP–PTR, the EVRP–PTR coordinates two transport modes: electric on-demand shuttle buses and public transport, represented in this study by the railway system. A set of customers (passengers), each located at distinct pickup points in the network, constitutes the target group of this coordination, aiming to reduce their total travel and waiting times from the origin location until boarding the railway service.

In the EVRP–PTR setting, electric shuttle buses may (re)charge at publicly accessible opportunity charging stations within the service area. Incorporating charging decisions into the VRP–PTR formulation transforms the problem into three interdependent components: (i) vehicle routing, (ii) shuttle charging scheduling, and (iii) public transport rescheduling. The charging component ensures that shuttle state-of-charge (SOC) levels remain within admissible bounds, but also increases system complexity, as charging detours may affect passenger waiting times and service synchronization.

3.2. Mathematical program

In formulating this problem, the following assumptions are adopted: (1) on-demand shuttle buses can start their trips from multiple depots (i.e., metro, railway, bus, and tram stations), and terminate their trip at the same railway station; (2) all shuttle bus trips follow the shortest route to each assigned pickup point; (3) the travel times of the shuttle buses between different vertices of the transport network are known in advance; and (4) each passenger is served exactly once, thereby ensuring complete coverage of the assigned demand. To incorporate the electrification of the on-demand fleet, we make the following additional assumptions:

1. Each shuttle bus begins its on-demand service with a fully charged battery.
2. Each opportunity charging facility can be used by only one vehicle at a time.
3. The opportunity (re)charging of on-demand shuttles has a fixed duration.

For this model, we consider a directed graph $\mathcal{G} = (\mathcal{V} \cup C, \mathcal{A})$. The vertex set $\mathcal{V}$ is divided into two subsets: $\mathcal{O} \cup \mathcal{P}$, where $\mathcal{P}$ denotes the pickup locations of passenger requests for the on-demand service, indexed by $\langle 1, \ldots, p \rangle$. Each pickup vertex shares the same destination, hereafter referred to as the *main railway station*. The set $\mathcal{O}$ contains the shuttle route origin and destination nodes, including two copies of the main railway station, denoted by $\langle 0, p+1 \rangle$, to distinguish shuttle route departures from arrivals. The set C represents the opportunity charging physical locations available to the shuttle fleet, each accommodating at most one shuttle at a time. The arc set A contains all feasible shuttle movements, including start, end, and inter-task paths, and is defined as the union of the following arc subsets:

$$\mathcal{A} = \begin{cases} \mathcal{A}_1 = (o, j) & \forall o \in \mathcal{O} \setminus \{p+1\},\ \forall j \in \mathcal{P} \\ \mathcal{A}_2 = (i, j) & \forall i \in \mathcal{P},\ \forall j \in \mathcal{P} \setminus \{i\},\ i \neq j \\ \mathcal{A}_3 = (i, c) & \forall i \in \mathcal{P},\ \forall c \in C \\ \mathcal{A}_4 = (c, i) & \forall c \in C,\ \forall i \in \mathcal{P} \\ \mathcal{A}_5 = (i, p+1) & \forall i \in \mathcal{P} \\ \mathcal{A}_6 = (c, p+1) & \forall c \in C \end{cases}$$

For each on-demand shuttle bus $k \in \mathcal{K}$, the abovementioned arc set $\mathcal{A}$ defines all feasible route movements. Specifically, $\mathcal{A}_1$ contains arcs from shuttle origin points to all pickup locations, $\mathcal{A}_2$ arcs between different pickup locations, and $\mathcal{A}_3 - \mathcal{A}_4$ arcs connecting pickup and charging locations in both directions. Finally, $\mathcal{A}_5$ and $\mathcal{A}_6$ represent feasible return arcs from pickup and charging locations, respectively, to the main railway station. Since shuttle buses cannot travel directly from their starting points to a charging location, $\mathcal{A}_1$ only includes origin-to-pickup arcs. Overall, the set $\mathcal{A}$ captures all feasible routing and (re)charging movements required for passenger service.

In this model, each shuttle bus departs from a predefined starting point (depot), either the main railway station vertex 0 or another node in $\mathcal{O}$, serves a sequence of pickup locations in $\mathcal{P}$, may (re)charge at locations in C when necessary, and terminates at the main railway station vertex $p+1$, where passengers are dropped off. Let $\mathcal{K}$ denote the set of available on-demand shuttle buses. A key objective of the proposed framework is to coordinate the operation of electric on-demand shuttle buses with the railway timetable to facilitate efficient passenger transfers. To improve this synchronization, railway departures may be rescheduled to maintain competitive combined travel times relative to private vehicle use. The railway trips are fixed and pre-scheduled throughout the day and are assumed sufficient to allow passengers to board the first available train. These trips are represented by the set $\mathcal{R}$, where each trip $r \in \mathcal{R}$ departs at time $y_r \in \mathbb{R}_{\geq 0}$.

Fig. 1 illustrates the network $\mathcal{G}$ with four pickup nodes and two opportunity charging locations, depicting all feasible shuttle movements among the main railway station, additional shuttle origins $\{\mathcal{O}_1, \mathcal{O}_2\}$, pickup nodes $\mathcal{P} = \{i, i+1, j, j+1\}$, and pantograph chargers $C = \{C_1, C_2\}$, including all potential charging events.

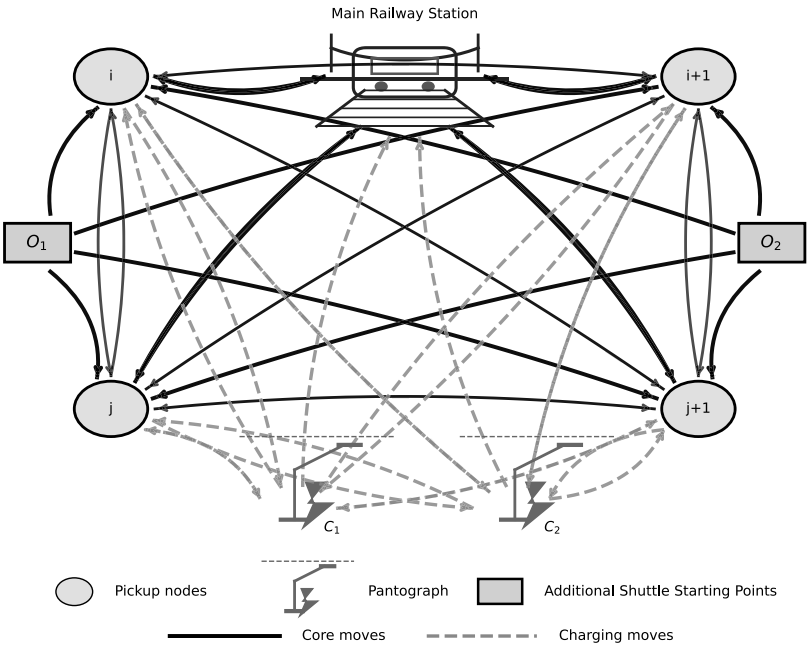

Fig. 1. Modeled representation of the network $\mathcal{G} = (\mathcal{V} \cup \mathcal{C}, \mathcal{A})$ of the electric on-demand shuttles $k \in \mathcal{K}$.

Each vertex $i \in \mathcal{V}$ is associated with a pickup demand $q_i \geq 0$, representing the number of passengers requesting on-demand service to access the most time-appropriate railway trip. Since shuttle buses depart from their origin points without passengers, $q_o = 0$ for all $o \in \mathcal{O} \setminus \{p+1\}$. Each pickup point $i \in \mathcal{P}$ is also associated with a requested pickup time $e_i \in \mathbb{R}_{\geq 0}$. Passenger boarding and alighting operations on the on-demand shuttle bus require a fixed service time $\beta \in \mathbb{R}_{\geq 0}$, while an additional fixed duration $\alpha \in \mathbb{R}_{\geq 0}$ is assumed for accessing the railway platform after alighting.

In terms of operational constraints, each shuttle bus $k \in \mathcal{K}$ is characterized by a maximum capacity $Q_k \in \mathbb{R}_{\geq 0}$ and a maximum operating time $\mathcal{T}_k \in \mathbb{R}_{\geq 0}$. Fleet size constitutes the primary operating cost component of the on-demand service. For each arc $(i, j) \in \mathcal{A}$, with $i, j \in \mathcal{V} \cup \mathcal{C}$, the direct shuttle travel time is denoted by $t_{ij} \in \mathbb{R}_{\geq 0}$, where $t_{ii} = +\infty$ excludes loops. Each electric shuttle is assumed to follow the shortest travel distance d_{ij} between consecutive locations (i, j). To maintain service quality, a maximum passenger waiting time $\mathcal{F} \in \mathbb{R}_{\geq 0}$ and a maximum in-vehicle ride time $\mathcal{L} \in \mathbb{R}_{\geq 0}$ are imposed. Finally, a tolerance parameter $s \in \mathbb{R}_{\geq 0}$ specifies the maximum allowable deviation from the scheduled railway timetable.

To account for fleet electrification, the state-of-charge (SOC) of each shuttle $k \in \mathcal{K}$ is constrained within predefined bounds $(SOC_k^{\min}, SOC_k^{\max})$, where $SOC_k^{\min}$ denotes the minimum allowable SOC and $SOC_k^{\max}$ the battery capacity of the vehicle. An intermediate threshold SOC_k^{up} is introduced to trigger opportunity charging before the SOC reaches the critical level $SOC_k^{\min}$. Battery consumption per unit distance is denoted by γ, while each charging event provides a fixed energy amount ΔH, assuming a constant charging duration ρ across all charging locations. The problem notation is summarized in Tables 2 and 3, with the latter presenting the sets, parameters, and variables related to fleet electrification of the on-demand service.

Considering the presented nomenclature, the combined mathematical model of the EVRP–PTR problem developed in this study is described below. The EVRP–PTR problem involves two objective functions. The first objective (f_1), given in Eq. (1), seeks to minimize the overall door-to-rail travel time of passengers. This overall door-to-rail travel time consists of three components: (1) the waiting time for shuttle pickup (m_i), (2) the in-vehicle travel time from the pickup point to the main railway station (n_i), and (3) the waiting time at the main railway station until the departure of the next train (w_i). The second objective (f_2), shown in Eq. (2), aims to minimize the operational cost of the on-demand service by reducing the number of available shuttle buses. This is modeled through the binary variable z_k, where $z_k = 1$ if on-demand shuttle $k \in \mathcal{K}$ is assigned to at least one pickup point and $z_k = 0$ otherwise, as constrained by Eq. (3). Together, these objectives define a multi-objective optimization problem (MOOP).

$$(\tilde{Q}):$$

$$\min \sum_{i \in \mathcal{P}} (m_i + n_i + w_i) \tag{1}$$

$$\min \sum_{k \in \mathcal{K}} z_k \tag{2}$$

$$\text{s.t.:} z_k \geq x_{ij}^k \qquad \forall (i,j) \in \mathcal{A}, \forall k \in \mathcal{K} \tag{3}$$

$$x_{ij}^k \in \{0,1\} \qquad \forall (i,j) \in \mathcal{A}, \forall k \in \mathcal{K} \tag{4}$$

Table 2
Nomenclature.

Sets	
$\mathcal{P}$	set of all pickup vertices
$\mathcal{O}$	set of copies of the main railway station and shuttle origin nodes
$\mathcal{V}$	set of copies of the main railway station, shuttle origin nodes, and pickup vertices, where $\mathcal{V} = \mathcal{O} \cup \mathcal{P}$
$\mathcal{A}$	arc set of all feasible routes where the on-demand vehicle can travel
$\mathcal{K}$	set of the available on-demand shared vehicles (shuttle buses)
$\mathcal{R}$	set of all scheduled railway trips during an operational day
Parameters	
y_r	departure time of the scheduled railway trip $r \in \mathcal{R}$
q_i	pickup passenger demand at each vertex $i \in \mathcal{V}$ for the on-demand service
e_i	pickup demand time of each vertex $i \in \mathcal{V}$ for the on-demand service
β	fixed time for the boarding/alighting of each passenger to the shared vehicle
α	fixed time for reaching the railway station dock after the alighting process
Q_k	capacity of each shuttle bus $k \in \mathcal{K}$
$\mathcal{T}_k$	maximum allowable running time of a shuttle bus $k \in \mathcal{K}$
d_{ij}	minimum travel distance of a feasible arc $(i, j) \in \mathcal{A}$
t_{ij}	travel time of traversing a feasible arc $(i, j) \in \mathcal{A}$
$\mathcal{F}$	maximum allowable waiting time of passengers at the pickup vertex $i \in \mathcal{P}$ until their pickup time by the on-demand service
$\mathcal{L}$	maximum allowable ride time of passengers from any pickup vertex $i \in \mathcal{P}$
s	the allowed timetable deviation for railway trips $r \in \mathcal{R}$
M	a very large positive number
Variables	
x_{ij}^k	$x_{ij}^k \in \{0, 1\}$, where $x_{ij}^k = 1$ if the on-demand shuttle bus $k \in \mathcal{K}$ serves vertices $(i, j) \in \mathcal{A}$ sequentially, and $x_{ij}^k = 0$ if not
θ_i^k	$\theta_i^k \in \{0, 1\}$, where $\theta_i^k = 1$ if the on-demand shuttle bus $k \in \mathcal{K}$ serves vertex $i \in \mathcal{V} \cup C$, and $\theta_i^k = 0$ if not
l_{ir}	$l_{ir} \in \{0, 1\}$, where $l_{ir} = 1$ if the passengers from pickup point $i \in \mathcal{P}$ are assigned to the railway trip $r \in \mathcal{R}$, and $l_{ir} = 0$ if not
z_k	$z_k \in \{0, 1\}$, where $z_k = 1$ if the on-demand shuttle bus $k \in \mathcal{K}$ serves at least one pickup vertex $i \in \mathcal{P}$, and $z_k = 0$ if not
u_i^k	$u_i^k \in \mathbb{R}_{\geq 0}$, indicating the actual time at which shuttle bus $k \in \mathcal{K}$ starts servicing vertex $i \in \mathcal{V} \cup C$
g_j^k	$g_j^k \in \mathbb{R}_{\geq 0}$, indicating the time at which shuttle bus $k \in \mathcal{K}$ starts servicing vertex $j \in \mathcal{V} \cup C$, considering the time it served the previous vertex $i : i \neq j, (i, j) \in \mathcal{A}$
τ_k	$\tau_k \in \mathbb{R}_{\geq 0}$, indicating the return time of the on-demand shuttle bus $k \in \mathcal{K}$ at the main railway station after unloading all serviced passengers from the pickup vertices
b_i	$b_i \in \mathbb{R}_{\geq 0}$, indicating the arrival time of passengers from pickup vertex $i \in \mathcal{P}$ at the main railway station
h_r	$h_r \in \mathbb{R}$, indicating the permitted timetable modifications for a railway trip $r \in \mathcal{R}$
m	$m = [m_1, \ldots, m_i, \ldots, m_{\lvert P \rvert}]^\intercal \in \mathbb{R}_{\geq 0}$, waiting time for the passenger demand $i \in \mathcal{P}$ from when the on-demand service is requested until the passenger demand is picked up
n	$n = [n_1, \ldots, n_i, \ldots, n_{\lvert P \rvert}]^\intercal \in \mathbb{R}_{\geq 0}$, in-vehicle travel time for the passenger demand $i \in \mathcal{P}$ corresponding to the $(i, p+1)$ request
w	$w = [w_1, \ldots, w_i, \ldots, w_{\lvert P \rvert}]^\intercal \in \mathbb{R}_{\geq 0}$, waiting time for the passenger demand $i \in \mathcal{P}$ from its arrival at the main railway station until the departure time of the next closest railway trip $r \in \mathcal{R}$

Table 3
Nomenclature for the opportunity-charging process of the electric on-demand shuttles.

Sets	
C	set of all physical sites for opportunity charging
Parameters	
$SOC_k^{\min}$	minimum allowed state-of-charge of shuttle bus $k \in \mathcal{K}$
$SOC_k^{\max}$	maximum allowed state-of-charge of shuttle bus $k \in \mathcal{K}$
SOC_k^{up}	the upper limit of the SOC interval $[SOC_k^{\min}, SOC_k^{up}]$ at which shuttle bus $k \in \mathcal{K}$ must visit a charging point (pantograph)
γ	battery consumption per traveled distance
ΔH	fixed energy added per visit to a charging point (pantograph)
ρ	fixed opportunity-charging duration
Variables	
δ_{kj}	$\delta_{kj} \in \{0, 1\}$, where $\delta_{kj} = 1$ if the on-demand shuttle bus $k \in \mathcal{K}$ is assigned for opportunity charging $j \in C$, and 0 otherwise
$\overline{SOC_k^i}$	$\overline{SOC_k^i} \in \mathbb{R}_{\geq 0}$, indicating the SOC of shuttle bus $k \in \mathcal{K}$ when leaving vertex $i \in \mathcal{V} \cup C$
SOC_k^i	$SOC_k^i \in \mathbb{R}_{\geq 0}$, indicating the SOC of shuttle bus $k \in \mathcal{K}$ when it arrives at vertex $i \in \mathcal{V} \cup C$
f_{kj}	$f_{kj} \in \mathbb{R}_{\geq 0}$, time at which shuttle bus $k \in \mathcal{K}$ begins opportunity charging at charging vertex $j \in C$
λ_{kj}	$\lambda_{kj} \in \mathbb{R}_{\geq 0}$, time at which shuttle bus $k \in \mathcal{K}$ completes opportunity charging at charging vertex $j \in C$
κ_{kj}	$\kappa_{kj} \in \mathbb{R}_{\geq 0}$, energy added (kWh) to a shuttle bus $k \in \mathcal{K}$ at vertex $j \in \mathcal{V} \cup C$; $\kappa_{kj} = 0$ if $j \in \mathcal{V}$ (no charger available), and $\kappa_{kj} > 0$ when $j \in C$ (charging vertex - pantograph)

$$z_k \in \{0,1\} \qquad \forall k \in \mathcal{K} \tag{5}$$

$$m_i, n_i, w_i \in \mathbb{R}_{\geq 0} \qquad \forall i \in \mathcal{P} \tag{6}$$

Constraints (7)–(11) are imposed to ensure route feasibility, flow conservation, and the efficient coverage of passenger demand by the on-demand service. Specifically, constraints (7) ensure that every pickup point $i \in \mathcal{P}$ with an active on-demand request is visited exactly once by a shuttle, guaranteeing complete demand coverage. This condition is expressed through the three-index decision variable x_{ij}^k, which takes the value 1 if shuttle bus $k \in \mathcal{K}$ travels directly from a pickup vertex $i \in \mathcal{P}$ to vertex $j \in \mathcal{V} \cup C$. Constraints (8) impose a round-trip structure for each shuttle bus: once a shuttle bus departs from its starting point to serve a pickup point $j \in \mathcal{P}$, it must eventually return to the main railway station after completing its assigned service, while maintaining its battery level within admissible limits. Constraints (9) and (10) restrict each on-demand shared vehicle to a single route, and ensure that the shuttle bus departs from its origin point whenever $x_{ij}^k = 1$ for an arc $(i,j) \in \mathcal{A}$. Constraints (11) establish flow continuity by ensuring that if a shuttle bus arrives at a pickup or charging node $g \in \mathcal{P} \cup C$, it must also depart from that node.

$$\sum_{k \in \mathcal{K}} \sum_{j:(i,j)\in\mathcal{A}} x_{ij}^k = 1 \qquad \forall i \in \mathcal{P} \tag{7}$$

$$\sum_{j:(o,j)\in\mathcal{A} \mid o\in\mathcal{O}\setminus\{p+1\}} x_{oj}^k = \sum_{j:(j,p+1)\in\mathcal{A}} x_{jp+1}^k \qquad \forall k \in \mathcal{K} \tag{8}$$

$$\sum_{i:(o,i)\in\mathcal{A} \mid o\in\mathcal{O}\setminus\{p+1\}} x_{oi}^k \leq 1 \qquad \forall k \in \mathcal{K} \tag{9}$$

$$\sum_{i:(o,i)\in\mathcal{A} \mid o\in\mathcal{O}\setminus\{p+1\}} x_{oi}^k \geq \sum_{i:(i,j)\in\mathcal{A}} \sum_{j\in\mathcal{P}} x_{ij}^k \qquad \forall k \in \mathcal{K} \tag{10}$$

$$\sum_{i:(i,g)\in\mathcal{A}} x_{ig}^k - \sum_{j:(g,j)\in\mathcal{A}} x_{gj}^k = 0 \qquad \forall g \in \mathcal{P} \cup C, \forall k \in \mathcal{K} \tag{11}$$

Constraints (12) impose capacity restrictions on the shuttle buses, preventing overload during pickups and ensuring that vehicle capacity is respected throughout the route. Constraints (13) are crucial for mapping shuttle buses to the vertices $i \in \mathcal{V} \cup C$ through the two-index binary variable θ_i^k, formulated using the big-M approach. In this model, M is defined as a very large positive constant ($M \ggg 0$), ensuring that θ_i^k is set to 1 whenever $x_{ij}^k = 1$ by satisfying the lower bound of the constraint.

$$\sum_{i\in\mathcal{P}} \sum_{j:(i,j)\in\mathcal{A}} q_i x_{ij}^k \leq Q_k \qquad \forall k \in \mathcal{K} \tag{12}$$

$$\frac{1}{M} \sum_{j:(i,j)\in\mathcal{A}} x_{ij}^k \leq \theta_i^k \leq \sum_{j:(i,j)\in\mathcal{A}} x_{ij}^k \qquad \forall i \in \mathcal{V} \cup C, \forall k \in \mathcal{K} \tag{13}$$

$$\theta_i^k \in \{0,1\} \qquad \forall i \in \mathcal{V} \cup C, \forall k \in \mathcal{K} \tag{14}$$

Constraints (15) ensure that the service time u_i^k of pickup point $i \in \mathcal{P}$ by shuttle bus $k \in \mathcal{K}$ is no earlier than the requested time instance e_i. Constraints (16) determine the exact departure time of shuttle bus k from its starting point, u_o^k, when the shuttle bus is assigned to serve pickup point i (i.e., $x_{oi}^k = 1$). This time is computed as $u_o^k = u_i^k - t_{oi}$, namely the difference between the service time at pickup point i and the travel time from the origin point to i. As will be shown in the subsequent Eq. (28) and (29), u_i^k is closely linked not only to e_i, but also to the potential completion time of any charging operation performed immediately after visiting i. This dependency is therefore incorporated into the computation of u_o^k, ensuring that any en-route charging activity of the shuttle bus is explicitly accounted for.

$$u_i^k \geq e_i \qquad \forall i \in \mathcal{P}, \forall k \in \mathcal{K} \tag{15}$$

$$u_o^k = u_i^k - t_{oi} \mid x_{oi}^k = 1 \qquad \forall o \in \mathcal{O} \setminus \{p+1\}, \forall i \in \mathcal{P}, \forall k \in \mathcal{K} \tag{16}$$

$$u_i^k \in \mathbb{R}_{\geq 0} \qquad \forall i \in \mathcal{V} \cup C, \forall k \in \mathcal{K} \tag{17}$$

Each on-demand shuttle bus $k \in \mathcal{K}$ begins daily operations fully charged, i.e., $SOC_k^o = SOC_k^{\max}$, as imposed by constraints (18). When the shuttle visits a node $j \in \mathcal{V} \cup C$, we distinguish the arrival state-of-charge, SOC_k^j, from the departure state-of-charge, $\overline{SOC_k^j}$. These are related by $\overline{SOC_k^j} = SOC_k^j + \kappa_k^j$, through constraints (19), where κ_k^j denotes the energy added to vehicle k at node j. Constraints (20) restrict κ_k^j to zero at non-charging nodes ($j \in \mathcal{V}$) and allow to be positive at charging nodes ($j \in C$) upon the execution of an opportunity charging. Specifically, at charging nodes, we define $\kappa_{kj} = \Delta H \delta_{kj}$, such that the battery receives a fixed energy amount ΔH whenever a charging operation is performed, with the binary variable δ_{kj} indicating whether shuttle bus k charges at node j. The state-of-charge dynamics of the shuttle bus along the route are given by constraints (21). Namely, for any active arc (i,j) with $x_{ij}^k = 1$, the arrival state-of-charge at node $j \in \mathcal{V} \cup C$, SOC_k^j, equals the departure state-of-charge from the preceding node i, $\overline{SOC_k^i}$, reduced by the energy consumption on arc (i,j), i.e., γd_{ij}.

To regulate (re)charging decisions, constraints (22) require the departure state-of-charge $\overline{SOC_k^j}$ of a shuttle bus $k \in \mathcal{K}$ at pickup node $j \in \mathcal{V}$ to remain above the threshold SOC_k^{up}, ensuring sufficient battery levels after servicing a pickup point. Constraints (23) further bound the arrival state-of-charge at charging locations according to $SOC_k^{\min} \leq SOC_k^j \leq SOC_k^{up}$, thereby defining the admissible

SOC range within which (re)charging operations may occur. Collectively, constraints (19) – (23), together with the binary variable δ_{kj}, determine when (re)charging takes place, and ensure that, whenever charging occurs, shuttle bus k departs charging node $j \in C$ with an additional energy amount κ_{kj}. Constraints (24) define the charging start time of shuttle bus k at charger j, denoted by f_{kj}, as the sum of the service completion time at the immediately preceding node i, u_i^k, with $(i,j) \in \mathcal{A}$, the passenger boarding duration at node i, $\beta q_i \theta_i^k$, and the travel time t_{ij}. This constraint becomes active only when shuttle bus k traverses arc (i,j), i.e., $x_{ij}^k = 1$, and a charging operation is scheduled at node j, i.e., $\delta_{kj} = 1$. Given f_{kj}, constraints (25) determine the charging completion time, λ_{kj}, as $f_{kj} + \rho$, where ρ denotes the fixed charging duration common to all shuttles and applies whenever $\delta_{kj} = 1$.

Opportunity charging sites can be used multiple times per day without predefined charging time slots. Consequently, the charging start time of each bus $k \in \mathcal{K}$ at charger $j \in C$, denoted by f_{kj}, may take any nonnegative continuous value at any opportunity charging location. This operational flexibility introduces the risk of overlapping charging sessions among multiple on-demand shuttle buses at the same charger. To prevent such conflicts, constraints (26) ensure that no charger is simultaneously occupied by more than one shuttle bus. In particular, if another on-demand vehicle $\phi \in \mathcal{K} \setminus \{k\}$ is assigned to charger j and initiates charging no later than shuttle bus $k \in \mathcal{K}$ (i.e., $f_{\phi j} \le f_{kj}$), then shuttle bus k cannot charge at the same location if its charging start time, f_{kj}, precedes ϕ's charging completion time, $\lambda_{\phi j}$. Equivalently, if the charging intervals $[f_{\phi j}, \lambda_{\phi j})$ and $[f_{kj}, \lambda_{kj})$ overlap, at most one of the corresponding charging decisions may be active, i.e., $\delta_{\phi j} + \delta_{kj} \le 1$. Constraints (27) further couple charging decisions with routing decisions by ensuring that shuttle bus k may charge at node $j \in C$ (i.e., $\delta_{kj} = 1$) only if it traverses an incoming arc from a pickup node $i \in \mathcal{P}$, such that $(i,j) \in \mathcal{A}$ and $x_{ij}^k = 1$.

To maintain the proper time sequence between consecutive visits, constraints (28) calculate the service-start time g_j^k at node $j \in \mathcal{V} \cup \mathcal{C}$ for shuttle bus $k \in \mathcal{K}$. For pickup nodes $j \in \mathcal{V}$, g_j^k is computed as the sum of the service time at the preceding node i, u_i^k, with $(i,j) \in \mathcal{A}$, the passenger boarding duration at node i, $\beta q_i \theta_i^k$, and the travel time t_{ij}, whenever shuttle bus k traverses arc (i,j) (i.e., $x_{ij}^k = 1$). This formulation also determines g_{p+1}^k, representing the time at which shuttle bus k returns to the main railway station after completing its assigned route. For charging nodes $j \in C$, g_j^k is equal to the charging completion time, λ_{kj}. Constraints (29), together with constraints (15), define the actual service time at pickup nodes $j \in \mathcal{P}$, u_j^k, as the maximum of g_j^k and the requested pickup time e_j, while for charging nodes $j \in C$, it holds that $u_j^k = g_j^k$.

$$SOC_k^o = SOC_k^{\max} \qquad \forall o \in \mathcal{O} \setminus \{p+1\}, \forall k \in \mathcal{K} \tag{18}$$

$$\overline{SOC_k^j} = SOC_k^j + \kappa_{kj} \qquad \forall j \in \mathcal{V} \cup C, \forall k \in \mathcal{K} \tag{19}$$

$$\kappa_{kj} = \begin{cases} 0, & \forall j \in \mathcal{V}, \forall k \in \mathcal{K} \\ \Delta H \delta_{kj}, & \forall j \in C, \forall k \in \mathcal{K} \end{cases} \tag{20}$$

$$SOC_k^j = (\overline{SOC_k^i} - \gamma d_{ij}) x_{ij}^k \qquad \forall (i,j) \in \mathcal{A} : j \in \mathcal{V} \cup C, \forall k \in \mathcal{K} \tag{21}$$

$$\overline{SOC_k^j} \ge SOC_k^{up} \qquad \forall j \in \mathcal{V}, \forall k \in \mathcal{K} \tag{22}$$

$$SOC_k^{\min} \le SOC_k^j \le SOC_k^{up} \mid \delta_{kj} = 1 \qquad \forall j \in C, \forall k \in \mathcal{K} \tag{23}$$

$$f_{kj} = (u_i^k + \beta q_i \theta_i^k + t_{ij}) x_{ij}^k \delta_{kj} \qquad \forall (i,j) \in \mathcal{A} : j \in C, \forall k \in \mathcal{K} \tag{24}$$

$$\lambda_{kj} = (f_{kj} + \rho) \delta_{kj} \qquad \forall j \in C, \forall k \in \mathcal{K} \tag{25}$$

$$\delta_{\phi j} + \delta_{kj} \le 1 \text{ if } f_{\phi j} \le f_{kj} \wedge f_{kj} < \lambda_{\phi j} \qquad \forall k \in \mathcal{K}, \forall \phi \in \mathcal{K} \setminus \{k\}, \forall j \in C \tag{26}$$

$$\delta_{kj} \ge x_{ij}^k \qquad \forall (i,j) \in \mathcal{A} : j \in C, \forall k \in \mathcal{K} \tag{27}$$

$$g_j^k = \begin{cases} u_i^k + \beta q_i \theta_i^k + t_{ij} \mid x_{ij}^k = 1, & \forall (i,j) \in \mathcal{A} : j \in \mathcal{V}, \forall k \in \mathcal{K} \\ \lambda_{kj}, & \forall j \in C, \forall k \in \mathcal{K} \end{cases} \tag{28}$$

$$u_j^k \begin{cases} \ge g_j^k, & \forall j \in \mathcal{V}, \forall k \in \mathcal{K} \\ = g_j^k, & \forall j \in C, \forall k \in \mathcal{K} \end{cases} \tag{29}$$

$$\delta_{kj} \in \{0,1\} \qquad \forall j \in C, \forall k \in \mathcal{K} \tag{30}$$

$$\kappa_{kj} \in \mathbb{R}_{\ge 0} \qquad \forall k \in \mathcal{K}, \forall j \in \mathcal{V} \cup C \tag{31}$$

$$g_j^k \in \mathbb{R}_{\ge 0} \qquad \forall j \in \mathcal{V} \cup C, \forall k \in \mathcal{K} \tag{32}$$

Constraints (33) define the first component of the door-to-rail passenger travel time, m_i, representing the passenger waiting time between the pickup request time e_i and the actual pickup time u_i^k by shuttle bus $k \in \mathcal{K}$. Constraints (34) ensure that this waiting time does not exceed the maximum allowable passenger threshold, $\mathcal{F}$, thereby supporting service quality and reliability. Constraints (35) determine the return time of shuttle bus k to the main railway station, τ_k, as the sum of its station arrival time, g_{p+1}^k, and the unloading duration associated with the served passenger demand, $\beta \sum_{i \in \mathcal{P}} q_i \theta_i^k$. In addition, constraints (36) enforce the maximum operating time $\mathcal{T}_k$ for each shuttle bus, measured as the elapsed time between its departure from the origin point, u_o^k, and its return to the main railway station, g_{p+1}^k. Constraints (37) define the passenger arrival time at the main railway station as $b_i = \tau_k + \alpha$ (whenever passenger demand i is served by shuttle bus k), where α denotes the estimated walking time from shuttle alighting to the railway platform.

Constraints (38) define the second component of the door-to-rail passenger travel time, n_i, representing the in-vehicle travel time of passenger demand $i \in \mathcal{P}$, computed as the difference between the passenger arrival time at the main railway station, b_i, and the corresponding pickup time by shuttle bus $k \in \mathcal{K}$, u_i^k. Constraints (39) ensure that the in-vehicle travel time does not exceed the maximum allowable threshold $\mathcal{L}$, thereby limiting excessive shuttle detours and promoting more efficient route selection within the underlying Vehicle Routing Problem (VRP) framework. Constraints (40) assign each pickup point to exactly one railway trip $r \in \mathcal{R}$, whose departure time may be rescheduled by an amount h_r within the allowable deviation range defined by constraints (41) and the predefined timetable flexibility parameter s. Constraints (42) then adjust the railway departure time, $y_r + h_r$, to better synchronize railway departures with the arrival time of the assigned passenger demand at the main railway station, b_i. Finally, constraints (43) define the third component of the door-to-rail passenger travel time, w_i, representing passenger waiting time at the railway station, calculated as the difference between the passenger arrival at the station, b_i, and the departure time of the next closest—potentially rescheduled—railway trip.

$$m_i = u_i^k - e_i \qquad \forall i \in \mathcal{P}, \forall k \in \mathcal{K} \tag{33}$$
$$m_i \leq \mathcal{F} \qquad \forall i \in \mathcal{P} \tag{34}$$
$$\tau_k = g_{p+1}^k + \beta \sum_{i \in \mathcal{P}} q_i \theta_i^k \qquad \forall k \in \mathcal{K} \tag{35}$$
$$g_{p+1}^k - u_o^k \leq \mathcal{T}_k \qquad \forall o \in \mathcal{O} \setminus \{p+1\}, \forall k \in \mathcal{K} \tag{36}$$
$$b_i = \tau_k + \alpha \mid \theta_i^k = 1 \qquad \forall i \in \mathcal{P}, \forall k \in \mathcal{K} \tag{37}$$
$$n_i = b_i - u_i^k \qquad \forall i \in \mathcal{P}, \forall k \in \mathcal{K} \tag{38}$$
$$n_i \leq \mathcal{L} \qquad \forall i \in \mathcal{P} \tag{39}$$
$$\sum_{r \in \mathcal{R}} l_{ir} = 1 \qquad \forall i \in \mathcal{P} \tag{40}$$
$$-s \leq h_r \leq s \mid l_{ir} = 1 \qquad \forall i \in \mathcal{P}, \forall r \in \mathcal{R} \tag{41}$$
$$(y_r + h_r) l_{ir} \geq b_i \qquad \forall i \in \mathcal{P}, \forall r \in \mathcal{R} \tag{42}$$
$$w_i = (y_r + h_r) - b_i \mid l_{ir} = 1 \qquad \forall i \in \mathcal{P}, \forall r \in \mathcal{R} \tag{43}$$
$$l_{ir} \in \{0, 1\} \qquad \forall i \in \mathcal{P}, \forall r \in \mathcal{R} \tag{44}$$
$$\tau_k \in \mathbb{R}_{\geq 0} \qquad \forall k \in \mathcal{K} \tag{45}$$
$$b_i \in \mathbb{R}_{\geq 0} \qquad \forall i \in \mathcal{P} \tag{46}$$
$$h_r \in \mathbb{R} \qquad \forall r \in \mathcal{R} \tag{47}$$

The nature of the proposed problem is multi-objective, as improving one objective (i.e., reducing the number of available shuttle buses) may deteriorate the other (i.e., increasing door-to-rail passenger travel time), and vice versa. To solve this multi-objective optimization problem (MOOP), we employ the ϵ-constraint solution method, which generates a representative subset of the Pareto front—the set of Pareto-optimal solutions capturing the best trade-offs between competing objectives. The ϵ-constraint approach is adopted because it efficiently yields a representative subset of the Pareto front—which, in most cases, is sufficient (Gkiotsalitis, 2023)—while remaining compatible with the exact solution requirements of the proposed mathematical program. Under this approach, objective function (2) is reformulated as a constraint by limiting the total number of utilized on-demand shuttle buses through a user-defined threshold, ϵ, while objective function (1) remains the primary optimization objective. With this consideration, objective function (2) is reformulated into the following constraints.

$$\sum_{k \in \mathcal{K}} z_k \leq \epsilon \qquad \epsilon \in \mathbb{Z}_{\geq 0} \tag{48}$$

By varying the value of ϵ and repeatedly solving the model for each corresponding threshold, the ϵ-constraint method generates a family of solutions, thereby acting as an *a posteriori* generator of Pareto-optimal solutions (Gkiotsalitis, 2023).

Mathematical program ($\tilde{Q}$) is non-convex due to nonlinearities in constraints (16), (21), (23) – (26), (28a), (37), and (41) – (43). In particular, these nonlinear constraints induce a non-convex feasible region, which complicates the search for globally optimal solutions. In our problem, most nonlinearities arise from logical expressions, whereas constraints (21), (24) – (25), and (42) contain products of decision variables. To address this, we linearize the nonlinear constraints using standard reformulation techniques and the big-M approach. In this method, M is set as a very large positive constant ($M \to +\infty$), as in constraints (13), so as to dominate the relevant terms and enable the intended activation or relaxation of the corresponding constraints. The adopted linearization procedures and the resulting auxiliary linear constraints are presented in detail in Appendix A. Based on these reformulations, mathematical program ($\tilde{Q}$) can be expressed as the following mixed-integer linear program (MILP), ($\hat{Q}$):

$$(\hat{Q}): \quad \min \quad \sum_{i \in \mathcal{P}} (m_i + n_i + w_i) \tag{49}$$

s.t.: Equations (3) – (15), (17) – (20), (22), (27), (28b) – (36), (38) – (40),

(44) – (48), (A.1) – (A.23), (A.25) – (A.29). (50)

Theorem 1. *Given that the problem is feasible, the continuous relaxation of the mathematical program* $(\hat{Q})$ *possesses a globally optimal solution.*

Proof. The mathematical program $(\hat{Q})$ in Eqs. (3) – (15), (17) – (20), (22), (27), (28b) – (36), (38) – (40), (44) – (48), (A.1) – (A.23), (A.25) – (A.29) is a mixed-integer linear program (MILP). Its continuous relaxation yields a feasible region described by affine equalities and inequalities, that is, a polyhedron. Since the objective function is linear, the relaxation is both convex and concave. Consequently, any local optimum of the relaxed problem is also a global optimum. □

According to Theorem 1, the mixed-integer linear program $(\hat{Q})$ can be solved to global optimality using exact MILP algorithms. This formulation ensures that, for any fixed ϵ-value within the ϵ-constraint multi-objective optimization framework, a globally optimal solution to the Electric Vehicle Routing and Public Transport Rescheduling Problem (EVRP–PTR) can be obtained.

4. Electric vehicle routing and public transport rescheduling problem under travel-time uncertainties

During daily operations, electric on-demand shuttle buses may experience travel-time variability due to traffic congestion, road incidents, roadworks, and adverse weather conditions, which can disrupt vehicle operations and delay passenger pickups. It is therefore important to account for such uncertainty in the decision-making process. In the remainder of this section, we consider stochastic travel times for traversing each feasible arc $(i, j) \in \mathcal{A}$, denoted by t_{ij}.

To capture this travel-time uncertainty, the deterministic parameter t_{ij} is replaced by a set of scenario-dependent values $t_{1,ij}, t_{2,ij}, \ldots, t_{|S|,ij}$ for each $(i, j) \in \mathcal{A}$, where S denotes the set of travel-time scenarios. A common way to address uncertainty is to optimize the expected value of the objective function, which requires probabilistic knowledge of the uncertain parameters, here represented by shuttle travel times. Since t_{ij} affects multiple layers of the problem, uncertainty propagates to all time-dependent variables, including u_i^k, g_j^k, τ_k, b_i, m_i, n_i, w_i, f_{kj}, and λ_{kj}, as well as the associated binary variables introduced in the linearization process (Appendix A). These variables therefore become scenario-dependent, taking $|S|$ values through Eqs. (16), (24) – (25), (28) – (29), (33), (35), (37) – (38), and (43). Consequently, the three components of passenger door-to-rail travel time also become scenario-dependent, namely $(m_{1,i}, m_{2,i}, \ldots, m_{|S|,i})$, $(n_{1,i}, n_{2,i}, \ldots, n_{|S|,i})$, and $(w_{1,i}, w_{2,i}, \ldots, w_{|S|,i})$, for all $i \in \mathcal{P}$. The objective is therefore to minimize the expected total door-to-rail passenger travel time:

$$\mathbb{E}\left[\sum_{i\in\mathcal{P}}(m_i + n_i + w_i)\right] \tag{51}$$

which can be equivalently written as:

$$\sum_{i\in\mathcal{P}}\mathbb{E}\left[(m_i + n_i + w_i)\right] \tag{52}$$

To solve this Stochastic Optimization Problem, we employ the Sample Average Approximation (SAA) (Kim et al., 2015; Gkiotsalitis et al., 2022), which approximates the expected value of the objective function in Eq. (52) by computing its average over the travel-time scenarios, as follows:

$$\frac{1}{|S|}\left[\sum_{s\in S}\sum_{i\in\mathcal{P}}\left(m_{s,i} + n_{s,i} + w_{s,i}\right)\right] \tag{53}$$

Introducing scenario-dependent travel times $t_{s,ij}$ may lead to infeasibilities across multiple layers of the EVRP–PTR framework due to increased shuttle travel times under certain scenarios. In particular, infeasibilities may arise in: (i) service start times; (ii) shuttle charging schedules; (iii) passenger waiting times; (iv) shuttle operating times; (v) passenger in-vehicle travel times; and (vi) railway timetable adjustments aimed at synchronizing train departures with passenger arrival times at the main railway station. To maintain feasibility, violations may be permitted in a limited number of scenarios. However, service start time constraints (Eq. (15)) and charging scheduling constraints (Eq. (26)) must always hold, as passengers cannot be served before their requested pickup time and chargers cannot be occupied simultaneously by multiple vehicles. The remaining constraints may be relaxed in selected scenarios, allowing the thresholds $\mathcal{F}$, $\mathcal{T}_k$, and $\mathcal{L}$ to be exceeded, or passenger arrivals b_i to occur after the departure of the assigned train. In such cases, passengers may wait for a subsequent train or, if no later departure is available, miss the railway service.

Based on the above considerations, the stochastic formulation of $(\hat{Q})$, accounting for shuttle travel-time uncertainty, is formulated as follows:

$$(\hat{Q}):$$

$$\min \quad \frac{1}{|S|}\left[\sum_{s\in S}\sum_{i\in\mathcal{P}}\left(m_{s,i} + n_{s,i} + w_{s,i}\right)\right] \tag{54}$$

$$\text{s.t.:} \quad \text{Equations (3) – (14), (17) – (20), (22), (27), (28b) – (33), (35), (38), (40), (44) – (48), (A.1) – (A.18), (A.20) – (A.23), (A.26) – (A.29)} \tag{55}$$

$$C_{1,s,ik} = u^k_{s,i} - e_i \qquad \forall i \in \mathcal{P}, \forall k \in \mathcal{K}, \forall s \in \{1,\dots,S\} \tag{56}$$

$$\sum_{s\in\mathcal{S}} \Pr\left(C_{1,s,ik} \geq 0\right) \geq \xi|\mathcal{S}| \qquad \forall i \in \mathcal{P}, \forall k \in \mathcal{K} \tag{57}$$

$$C_{2,s,k\phi j} = \delta_{\phi j} + \delta_{kj} - [1 + M(1 - \mu_{s,k\phi j})]$$
$$\forall k \in \mathcal{K}, \forall \phi \in \mathcal{K} \setminus \{k\}, \forall j \in C, \forall s \in \{1,\dots,S\} \tag{58}$$

$$\sum_{s\in\mathcal{S}} \Pr\left(C_{2,s,k\phi j} \leq 0\right) \geq \xi|\mathcal{S}| \qquad \forall k \in \mathcal{K}, \forall \phi \in \mathcal{K} \setminus \{k\}, \forall j \in C \tag{59}$$

$$C_{3,s,i} = m_{s,i} - \mathcal{F} \qquad \forall i \in \mathcal{P}, \forall s \in \{1,\dots,S\} \tag{60}$$

$$\sum_{s\in\mathcal{S}} \Pr\left(C_{3,s,i} \leq 0\right) \geq \xi|\mathcal{S}| \qquad \forall i \in \mathcal{P} \tag{61}$$

$$C_{4,s,ko} = g^k_{s,p+1} - (u^k_{s,o} + \mathcal{T}_k)$$
$$\forall o \in \mathcal{O} \setminus \{p+1\}, \forall k \in \mathcal{K}, \forall s \in \{1,\dots,S\} \tag{62}$$

$$\sum_{s\in\mathcal{S}} \Pr\left(C_{4,s,ko} \leq 0\right) \geq \xi|\mathcal{S}| \qquad \forall o \in \mathcal{O} \setminus \{p+1\}, \forall k \in \mathcal{K} \tag{63}$$

$$C_{5,s,i} = n_{s,i} - \mathcal{L} \qquad \forall i \in \mathcal{P}, \forall s \in \{1,\dots,S\} \tag{64}$$

$$\sum_{s\in\mathcal{S}} \Pr\left(C_{5,s,i} \leq 0\right) \geq \xi|\mathcal{S}| \qquad \forall i \in \mathcal{P} \tag{65}$$

$$C_{6,s,ir} = (y_r + h_r) - b_{s,i} \qquad \forall i \in \mathcal{P}, \forall r \in \mathcal{R}, \forall s \in \{1,\dots,S\} \tag{66}$$

$$\sum_{s\in\mathcal{S}} \Pr\left(C_{6,s,ir} \geq 0\right) \geq \xi|\mathcal{S}| \qquad \forall i \in \mathcal{P}, \forall r \in \mathcal{R} \tag{67}$$

$$C_{1,s,ik}, C_{2,s,k\phi j}, C_{3,s,i}, C_{4,s,ko}, C_{5,s,i}, C_{6,s,ir} \in \mathbb{R} \qquad \forall i \in \mathcal{P}, \forall k \in \mathcal{K}, \forall \phi \in \mathcal{K} \setminus \{k\},$$
$$\forall j \in C, \forall o \in \mathcal{O} \setminus \{p+1\}, \forall r \in \mathcal{R}, \forall s \in \{1,\dots,S\} \tag{68}$$

$$\xi \in (0,1] \tag{69}$$

where constraints (56) – (69) extend the deterministic EVRP–PTR formulation by incorporating shuttle travel-time uncertainty, thereby replacing constraints (15), (34), (36), (39), (A.19), and (A.25). These constraints introduce the auxiliary variables $C_{1,s,ik}, C_{2,s,k\phi j}, C_{3,s,i}, C_{4,s,ko}, C_{5,s,i}$, and $C_{6,s,ir}$, which quantify deviations from the corresponding deterministic conditions under scenario-dependent shuttle travel times. Specifically, $C_{1,s,ik}$ measures the difference between the service time $u^k_{s,i}$ and the passenger request time e_i, while $C_{2,s,k\phi j}$ captures the linearized charging-conflict condition. Similarly, $C_{3,s,i}$, $C_{4,s,ko}$, and $C_{5,s,i}$ measure deviations from the passenger waiting time, shuttle operating time, and in-vehicle travel time thresholds ($\mathcal{F}$, $\mathcal{T}_k$, and $\mathcal{L}$), whereas $C_{6,s,ir}$ measures the difference between passenger arrival times at the main railway station, $b_{s,i}$ and the (potentially rescheduled) railway departure time $(y_r + h_r)$. Constraints (57), (59), (61), (63), (65), and (67) require these conditions to hold in at least a proportion $\xi(\%)$ of the shuttle travel-time scenarios $s \in \mathcal{S}$, with ξ applied consistently across all constraints.

These constraints therefore define the probability with which the stochastic conditions $C_{1,s,ik} \geq 0$, $C_{2,s,k\phi j} \leq 0$, $C_{3,s,i} \leq 0$, $C_{4,s,ko} \leq 0$, $C_{5,s,i} \leq 0$, and $C_{6,s,ir} \geq 0$ must hold across S. When $\xi = 1$, these constraints act as strict *stochastic constraints*, enforcing feasibility for all scenarios. Since this may be overly restrictive or even infeasible, controlled violations are allowed by requiring feasibility with high probability rather than certainty. Under this interpretation, the formulation adopts a *chance-constrained* structure, commonly used in uncertain combinatorial optimization and closely related to Stochastic Constraint Satisfaction Problems (SCSPs) (Zghidi et al., 2018). As noted above, constraints (57) and (59) must always hold ($\xi = 1$), since service-time feasibility and charging-conflict avoidance are essential for valid solutions. In contrast, constraints (61), (63), (65), and (67) may function either as strict stochastic or as chance constraints, permitting occasional violations while requiring feasibility with probability at least ξ.

To implement the satisfaction probability functions (57), (59), (61), (63), (65), and (67) within the mixed-integer linear EVRP–PTR framework, they are reformulated through constraints (B.1) – (B.20), presented in Appendix B, by introducing the binary variables $c_{1,s,ik}$, $c_{2,s,k\phi j}$, $c_{3,s,i}$, $c_{4,s,ko}$, $c_{5,s,i}$, and $c_{6,s,ir}$. These variables indicate whether the corresponding stochastic conditions are satisfied under each scenario. Specifically, $c_{1,s,ik} = 1$ when $C_{1,s,ik} \geq 0$, and 0 otherwise, thereby counting the scenarios in which this stochastic condition holds. Similarly, $c_{2,s,k\phi j}$, $c_{3,s,i}$, $c_{4,s,ko}$, $c_{5,s,i}$, and $c_{6,s,ir}$ equal 1 when $C_{2,s,k\phi j} \leq 0$, $C_{3,s,i} \leq 0$, $C_{4,s,ko} \leq 0$, $C_{5,s,i} \leq 0$, and $C_{6,s,ir} \geq 0$, respectively, and 0 otherwise.

When the satisfaction probability condition (67) is applied with $\xi < 1$, $C_{6,s,ir}$ may become negative in a subset of scenarios. Since this term corresponds to the passenger waiting time at the railway station, $w_{s,i}$, as defined in Eqs. (43) and (66), and constitutes the third component of the door-to-rail passenger travel time in objective function (54), it must remain non-negative. To ensure this, the objective function is modified as follows:

$$(\hat{Q}):$$
$$\min \frac{1}{|S|}\left[\sum_{s\in\mathcal{S}}\sum_{i\in\mathcal{P}}\left(m_{s,i} + n_{s,i} + \max\left\{w_{s,i}, 0\right\}\right)\right] \tag{70}$$

The inclusion of the $\max\{\cdot\}$ operator introduces nonlinearity. This can be eliminated by introducing the auxiliary continuous variable $\tilde{w}_{s,i} \in \mathbb{R}_{\geq 0}$ and the linear constraints (71) – (73).

$$\tilde{w}_{s,i} \geq (y_r + h_r) - b_{s,i} - M(1 - l_{ir}) \qquad \forall i \in \mathcal{P}, \forall r \in \mathcal{R}, \forall s \in \{1, \ldots, S\} \tag{71}$$

$$\tilde{w}_{s,i} \leq (y_r + h_r) - b_{s,i} + M(1 - l_{ir}) \qquad \forall i \in \mathcal{P}, \forall r \in \mathcal{R}, \forall s \in \{1, \ldots, S\} \tag{72}$$

$$\tilde{w}_{s,i} \geq 0 \qquad \forall i \in \mathcal{P}, \forall s \in \{1, \ldots, S\} \tag{73}$$

The auxiliary variable $\tilde{w}_{s,i}$ replaces the nonlinear term

$$\max\left\{w_{s,i}, 0\right\}$$

in the objective function, resulting in a mixed-integer linear programming formulation. The final EVRP–PTR framework, which accounts for stochastic shuttle travel-time parameters and can be solved to global optimality, is summarized as follows:

$$(\hat{Q}):$$

$$\min \frac{1}{|S|}\left[\sum_{s\in S}\sum_{i\in\mathcal{P}}\left(m_{s,i} + n_{s,i} + \tilde{w}_{s,i}\right)\right] \tag{74}$$

s.t.:Equations (3) – (14), (17) – (20), (22), (27), (28b) – (33), (35), (38), (40), (44) – (48), (56), (58), (60), (62), (64), (66), (68) – (69), (71) – (73), (A.1) – (A.18), (A.20) – (A.23), (A.26) – (A.29), (B.1) – (B.20).

However, this stochastic formulation introduces a significantly larger number of binary variables compared to its deterministic counterpart. More precisely, the number of additional binary variables grows proportionally with $|\mathcal{K}| \times |\mathcal{O}|, 2 \times |\mathcal{P}|$, $|\mathcal{P}| \times |\mathcal{R}|, |\mathcal{P}| \times |\mathcal{K}|$, and $|\mathcal{K}|^2 \times |C|$. As a result, the solution space and the size of the search tree increase substantially, rendering the stochastic problem computationally more demanding than the deterministic formulation.

5. Numerical experiments

5.1. Numerical experiments description

The proposed model is tested in two settings: (i) a toy network with synthetic data and (ii) a real-world network in Athens, Greece. In the Athens case study, pickup points span the Municipality of Athens and surrounding metropolitan areas. Opportunity-charging sites C are predefined along shuttle operating routes using existing trolleybus stops, selected to reflect the spatial distribution of demand across central and suburban zones, while enabling in-service (re)charging with minimal detours. Each charging site hosts a single pantograph for inductive wireless power transfer (WPT), following Doubleday et al. (2016). Although WPT infrastructure is typically deployed at fixed public transport (PT) stops, depots, or tramway DC grids to reduce infrastructure costs, particularly in dense urban areas (Shams Ashkezari et al., 2022; Elmenshawy and Massoud, 2022; Shams Ashkezari et al., 2024), depot charging is excluded here to prioritize fast, en-route charging.

Across all model applications, boarding and alighting time is fixed at $\beta = 7$ seconds per passenger (Jara-Díaz and Tirachini, 2013; AlHadidi and Rakha, 2019; Xue et al., 2022), while passenger access time from shuttle drop-off to the railway platform is set to $\alpha = 5$ minutes based on field observations. To ensure service quality, passenger waiting time at pickup points is limited to $\mathcal{F} = 20$ minutes and in-vehicle travel time to $\mathcal{L} = 45$ minutes. Railway trips $\mathcal{R}$ follow a typical Athens–Thessaloniki daily schedule, with rescheduling bounded by $s = 2$ minutes. The on-demand fleet $\mathcal{K}$ is constrained by an ϵ-value defining the maximum number of available vehicles. Each shuttle bus has a capacity of $Q_k = 13$ passengers (Sun and Zu, 2025) and a maximum operating duration of $\mathcal{T}_k = 55$ minutes. Operations begin at 6:00 a.m. and end after the final request or railway departure. Shuttle travel times t_{ij} are based on Euclidean distances in the toy network and shortest-path OpenStreetMap (OSM) distances in Athens, assuming an average speed of 30 km/h, consistent with off-peak statistics reported by the Athens Urban Transportation Organization (OASA).

Regarding electrification, Athens' new electric bus specifications (Abel, 2024) are adopted, whereby each shuttle operates within $SOC_k \in [20, 100]$ kWh, with an opportunity-charging threshold $SOC_k^{up} = 64$ kWh in the toy network and $SOC_k^{up} = 56$ kWh in the Athens case study. Average energy consumption is set to $\gamma = 2.80$ kWh/km, deliberately exceeding the observed maximum (~ 1.30 kWh/km in Athens, 2025) to account for worst-case energy demand. Each pantograph supplies $\Delta H = 18$ kWh within $\rho = 2.4$ minutes, consistent with flash pantograph systems (Shams Ashkezari et al., 2024; Elmenshawy and Massoud, 2022).

The following subsections present the implementation of the EVRP–PTR framework in both the toy and the Athens case study settings. For the Athens case study, additional analyses are conducted, including: (i) a computational performance analysis to assess the model's tractability; (ii) a sensitivity analysis of the Public Transport Rescheduling (PTR) component, examining two additional timetable deviations, $s = 0$ and $s = 1$ minute, relative to the initial case of $s = 2$ minutes, to evaluate the effect of railway timetable flexibility on passenger service quality, particularly in long-distance services where schedule adjustments may be more disruptive to passengers than in high-frequency urban PT systems (i.e., metro and tram services); (iii) a comparison with a baseline scenario in which railway timetable coordination with the on-demand service and opportunity charging are deactivated; (iv) an evaluation of the

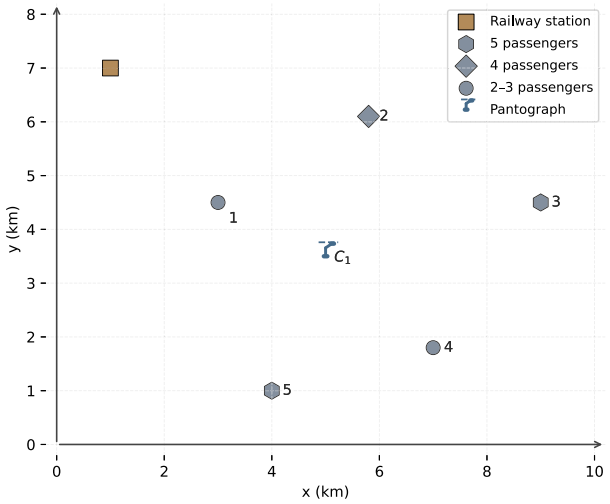

Fig. 2. Toy Network — Locations of the railway station, pantograph, and pickup points with the corresponding passenger demand in two dimensions.

on-demand service under travel-time uncertainty; and (v) a multi-origin shuttle scenario, assessing the applicability of the EVRP–PTR framework under shuttle operations with multiple starting points (depots).

All experiments are conducted using the mathematical formulations outlined in Sections 3 and 4. The model is implemented in Python 3.12 and solved with Gurobi 12.0.1 on a machine equipped with a 12th Gen Intel(R) Core(TM) i7-12700 CPU @ 2.30 GHz processor and 32 GB of RAM.

5.2. Travel-time scenarios for the on-demand service

During daily operations, electric on-demand services may experience variability in travel times between shuttle origin points, pickup vertices, opportunity charging locations, and the main railway station. Consequently, shuttle travel durations may vary substantially from day to day. This section presents the methodology used to generate travel-time scenarios that capture this variability within the proposed framework. Specifically, uncertain shuttle travel times are sampled from a probability distribution to realistically represent operating conditions.

Previous studies (El Faouzi and Maurin, 2007; Mazloumi et al., 2010; Rahman et al., 2018) suggest that bus travel times can be modeled using either normal or log-normal distributions, depending on data characteristics and variability patterns. Although both distributions are applicable, the log-normal distribution is adopted here because it ensures non-negative values and better captures the right-skewed nature commonly observed in travel-time data (Wang et al., 2012). Accordingly, uncertain shuttle travel times $t_{s,ij}$ are generated through log-normal sampling for the Athens case study, producing a representative set of travel-time scenarios.

Each model instance is solved under two satisfaction thresholds, $\xi = 90\%$ and $\xi = 100\%$, to evaluate different levels of constraint strictness. The case $\xi = 100\%$ represents a fully conservative setting, where the stochastic constraints in (B.3), (B.6), (B.9), (B.13), (B.16), and (B.20) enforce the conditions $C_{1,s,ik} \geq 0$, $C_{2,s,k\phi j} \leq 0$, $C_{3,s,i} \leq 0$, $C_{4,s,ko} \leq 0$, $C_{5,s,i} \leq 0$, and $C_{6,s,ir} \geq 0$ across all scenarios $s \in S$. In contrast, $\xi = 90\%$ implements chance constraints in (B.9), (B.13), (B.16), and (B.20), requiring the conditions $C_{3,s,i} \leq 0$, $C_{4,s,ko} \leq 0$, $C_{5,s,i} \leq 0$, and $C_{6,s,ir} \geq 0$ to hold in at least 90% of scenarios. As discussed in Section 4, constraints (57) and (59), together with their reformulations (B.3) and (B.6), must always hold ($\xi = 1$), since service-time feasibility and charging-conflict avoidance are essential for valid solutions. Therefore, chance constraints are not applied to them.

5.3. Demonstration of the toy network

In this subsection, the model is demonstrated on a toy network to clearly illustrate its inputs and outputs and facilitate reproducibility. The network comprises five pickup nodes ($|\mathcal{P}| = 5$) and 19 passengers representing exogenous demand for access to the railway station via the on-demand service. All shuttle buses are assumed to originate from the same location, namely the main railway station, where all routes terminate. Fig. 2 illustrates the network layout: the railway station is shown in the upper-left as a brown rectangle, pickup nodes $\mathcal{P} = \{\#1, \#2, \#3, \#4, \#5\}$ are distributed across the area, and a single opportunity charging point–pantograph, $C = \{C_1\}$, is located near the center. Charging may occur at any time within the planning horizon without predefined charging slots. However, simultaneous charging at the same pantograph is not allowed, implying that at most one shuttle bus may charge at a time. Pickup nodes are symbolically differentiated according to passenger demand.

Table 4 reports the travel times from vertex $i \in \mathcal{V} \cup C$ to vertex $j \in \mathcal{V} \cup C$. Vertices #0 and #6 denote the two copies of the railway station $\mathcal{O} = \{\#0, \#6\}$, which serve as the common origin and destination terminal for all on-demand shuttle buses. To forbid self-loops, we set $t_{ii} = +\infty$ for identical pickup vertices.

Table 4
Travel time t_{ij} from node $i \in \mathcal{V} \cup \mathcal{C}$ to node $j \in \mathcal{V} \cup \mathcal{C}$ (minutes).

O\D	0	1	2	3	4	5	6	$\mathcal{C}_1$
0	$+\infty$	6.40	9.77	16.76	15.88	13.42	$+\infty$	10.63
1	6.40	$+\infty$	6.45	12.00	9.65	7.28	6.40	4.47
2	9.77	6.45	$+\infty$	7.16	8.93	10.82	9.77	5.44
3	16.76	12.00	7.16	$+\infty$	6.72	12.21	16.76	8.25
4	15.88	9.65	8.93	6.72	$+\infty$	6.21	15.88	5.25
5	13.42	7.28	10.82	12.21	6.21	$+\infty$	13.42	5.39
6	$+\infty$	6.40	9.77	16.76	15.88	13.42	$+\infty$	10.63
$\mathcal{C}_1$	10.63	4.47	5.44	8.25	5.25	5.39	10.63	$+\infty$

Table 5
Passenger demand q_i and pickup demand time e_i (minutes past midnight) of each vertex $i \in \mathcal{P}$ for the on-demand service.

i	e_i	q_i
1	390	3
2	400	4
3	405	5
4	395	2
5	405	5
	Total:	**19**

Table 6
Scheduled times of railway trips (y_r) during the early-morning operational period (minutes past midnight).

r	1	2	3	4	5
y	405	420	435	450	465

For each pickup vertex $i \in \mathcal{P}$, passenger demand q_i and its corresponding requested pickup time e_i are reported in Table 5. Requests span a short interval—from 6:30 a.m. to 6:45 a.m.—to stress-test dispatching under tightly clustered demand. To evaluate synchronization with rail services, we consider $|\mathcal{R}| = 5$ scheduled railway trips (Table 6), concentrated in the early-morning period, with departures between 6:45 a.m. and 7:45 a.m. The compact railway schedule is intended to assess whether closely timed passenger requests can be effectively coordinated between the electric on-demand service and the railway system. The maximum on-demand fleet size varies over $\epsilon \in \{3, 4, 5\}$. Fleet sizes $|\mathcal{K}| \leq 2$ resulted in infeasible solutions, whereas $|\mathcal{K}| > 5$ was not considered given the small network size ($|\mathcal{P}| = 5$).

Using the ϵ-constraint method, the multi-objective EVRP–PTR problem was solved iteratively for each examined ϵ-value. In all cases, $\epsilon \in \{3, 4, 5\}$, the same Pareto-optimal solution was obtained. This globally optimal solution indicates that, at the toy-network scale, increasing the number of available shuttle buses beyond three does not further reduce the total door-to-rail passenger travel time. The resulting shuttle routes are listed below and illustrated in Fig. 3. All shuttle tours satisfy the maximum operating duration constraint $\mathcal{T}_k = 55$ minutes, while the total travel time of the utilized vehicles is 94.92 minutes. Notably, two of the three shuttles (#1 and #3) require an opportunity-charging stop at pantograph $\mathcal{C}_1$.

- On-demand shuttle bus #1 serving the task node sequence $0 \to 1 \to 3 \to \mathcal{C}_1 \to 6$
- On-demand shuttle bus #2 serving the task node sequence $0 \to 2 \to 6$
- On-demand shuttle bus #3 serving the task node sequence $0 \to 4 \to 5 \to \mathcal{C}_1 \to 6$

Table 7 summarizes the passenger-level outputs for the optimal three-shuttle solution. For each pickup vertex $i \in \mathcal{P}$, the passenger service time u_i^k exactly matches the requested pickup time e_i reported in Table 5; therefore, passengers incur no waiting at pickup locations ($m_i = 0$). Consequently, constraints (34), imposing $m_i \leq \mathcal{F} = 20$ minutes, are satisfied. In-vehicle ride times (n_i), reported in Table 7, remain below the maximum threshold $\mathcal{L} = 45$ minutes required by constraints (39). The table further reports passenger arrival times at the railway station (b_i) and rail-platform waiting times (w_i), which remain low, with a maximum value of 5.29 minutes. Accordingly, pickup waiting time m_i and rail waiting time w_i range between 0 and 5.29 minutes, indicating efficient coordination between the on-demand shuttle service and the railway system.

In contrast, passenger in-vehicle travel time n_i constitutes the dominant component of door-to-rail travel time, ranging from 15.73 to 40.69 minutes. The maximum value arises from the detour of shuttle #1 to pantograph $\mathcal{C}_1$ for an opportunity charge. This highlights a key trade-off in electric on-demand operations: while fleet electrification enhances environmental sustainability, charging detours may occasionally increase passenger travel time. The optimal objective value for the toy network is 155 minutes.

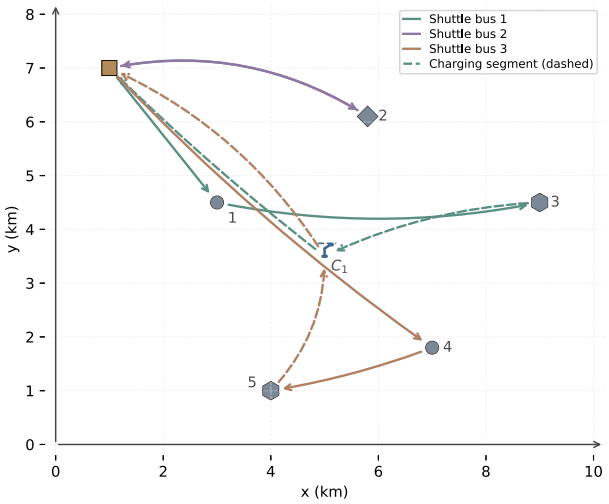

Fig. 3. Toy network solution — Optimal route paths of the three electric on-demand shuttles $k \in \mathcal{K}$.

Table 7
Service start time (u_i^k) (minutes past midnight), arrival time (b_i) (minutes past midnight) at the railway station, and total door-to-rail travel time ($m_i + n_i + w_i$) (minutes) for the passenger demand of each vertex $i \in \mathcal{P}$.

k	i	u_i^k	m_i	n_i	b_i	w_i
#1	1	390	0	40.69	430.69	2.31
	3	405	0	25.69		2.31
#2	2	400	0	15.73	415.73	2.27
#3	4	395	0	32.71	427.71	5.29
	5	405	0	22.71		5.29
Objective Function Value: 155 minutes						

Table 8
Passenger demand assignment of each pickup vertex $i \in \mathcal{P}$ to the railway schedules $r \in \mathcal{R}$, timetable railway trip modifications h_r (minutes), and modified railway trip schedules ($y_r + h_r$) (minutes past midnight).

i	r	h_r	$y_r + h_r$
1	3	-2.00	433
3			
2	2	-2.00	418
4	3	-2.00	433
5			

To further interpret railway waiting times w_i, Table 8 reports passenger assignments from pickup nodes $i \in \mathcal{P}$ to railway trips $r \in \mathcal{R}$, together with the timetable adjustments introduced to improve synchronization with the on-demand service. In particular, 15 of the 19 passengers are assigned to trip $r = 3$, originally scheduled at 7:15 a.m. and advanced by two minutes to 7:13 a.m. The remaining four passengers (from $i = 2$) are assigned to trip $r = 2$, rescheduled from 7:00 a.m. to 6:58 a.m. These minor timetable adjustments tighten passenger transfers and reduce railway waiting times w_i, while remaining within the allowable operational limits.

Table 9 reports, for each shuttle bus $k \in \mathcal{K}$ and vertex $j \in \mathcal{V} \cup C$, the arrival and departure state-of-charge (SOC_k^j, $\overline{SOC_k^j}$), together with the charging start and completion times (f_{kj}, λ_{kj}) at opportunity charging locations $j \in C$. Shuttles #1 and #3 arrive at pantograph C_1 with SOC levels—$SOC_1^{C_1} = 62.69$ kWh and $SOC_3^{C_1} = 61.54$ kWh—within the admissible range $[SOC_k^{\min}, SOC_k^{up}] = [20, 64]$ required by constraints (23). Upon charging, each shuttle receives the fixed energy increment $\Delta H = 18$ kWh. Shuttle #2 does not visit the charger, as its SOC never falls below SOC_k^{up}. All vehicles, including those charging at C_1, return to the railway station

Table 9
Arrival and departure SOC (SOC_k^j, $\overline{SOC_k^j}$) (in kWh) at vertex $j \in \mathcal{V} \cup C$, and charging start (f_{kj}) and completion (λ_{kj}) time values (minutes past midnight) at the opportunity-charger $j \in C$ of each electric shuttle $k \in \mathcal{K}$.

k	j	SOC_k^j	$\overline{SOC_k^j}$	f_{kj}	λ_{kj}
#1	1	91.04	91.04	–	–
	3	74.24	74.24	–	–
	C_1	62.69	80.69	413.85	414.10
	6	65.81	65.81	–	–
#2	2	86.33	86.33	–	–
	6	76.25	76.25	–	–
#3	4	77.77	77.77	–	–
	5	69.08	69.08	–	–
	C_1	61.54	79.54	410.99	411.24
	6	64.65	64.65	–	–

Table 10
Passenger demand q_i and requested pickup time e_i (minutes past midnight) for each pickup vertex $i \in \mathcal{P}$.

i	1	2	3	4	5	6	7	8	9	10	11	12	13	14	15	16	17	18	19	20
e_i	430	480	470	480	570	820	830	935	945	1050	1065	1035	1080	465	410	585	600	1405	1410	1395
q_i	6	7	7	6	4	6	7	8	5	6	5	7	8	6	7	5	4	7	3	3

with $SOC_k^6 > SOC_k^{up}$, confirming compliance with the energy constraints. Consistent with the single-charger requirement, charging intervals at pantograph C_1 remain non-overlapping, with shuttle #3 charging first.

Within this energy-management setting, the emergence of a single Pareto-optimal solution can be explained by the combined effect of the small network size, limited demand, and the SOC-based charging rules. At the toy-network scale, three shuttle buses are sufficient to serve all passengers while satisfying service and energy constraints. Adding more vehicles does not further reduce total door-to-rail passenger travel time, as routes are already sufficiently short. Moreover, constraints (23) permit charging only when $SOC_k^{\min} \le SOC_k^j \le SOC_k^{up}$, limiting unnecessary charger visits. As a result, alternative routing configurations with additional shuttle buses do not improve the objective and are either dominated or operationally redundant, yielding a single Pareto-optimal point.

5.4. Extended network — Athens case study

This case study uses real data from Athens, Greece. Larissa station serves as the central rail hub, hereafter referred to as the main railway station, while the Athens–Thessaloniki corridor constitutes the primary rail service. Passenger demand is transported to the railway station via on-demand electric shuttles. Fig. 4 presents the main railway station (Larissa station), pickup nodes, and opportunity-charging locations. It also depicts two additional shuttle origin points (depots), Dekelia station ($\mathcal{O}_1$) and Piraeus station ($\mathcal{O}_2$), which are further examined in the multi-origin shuttle scenario of Section 5.4.5. Specifically, Dekelia station serves as a railway station, while Piraeus station corresponds to a metro station. In the main Athens case study, however, all shuttle buses are assumed to originate from and return to Larissa station. Pickup points are distributed across central Athens and nearby municipalities, emphasizing areas where access to Larissa station typically requires multiple public transport transfers. In such cases, private vehicles, taxis, or on-demand shuttles provide more direct access to the station. Opportunity-charging locations are selected from existing trolleybus stops across the Athens metropolitan area, as described in Section 5.1. In total, five charging sites are considered, $C = \{C_1, C_2, C_3, C_4, C_5\}$, whose exact locations are shown in Fig. 4.

The extended study area comprises $|\mathcal{P}| = 20$ pickup points with a total number of 117 passengers. Service is provided by an on-demand shuttle fleet with sizes $|\mathcal{K}| = 12$ to $|\mathcal{K}| = 20$; these values play the role of the ϵ-constant parameter in constraints (48) across repeated runs. Instances with $|\mathcal{K}| < 12$ were infeasible because the fleet could not satisfy all pickup requests. For larger pickup sets ($|\mathcal{P}| > 20$), the model could not be solved within a reasonable time on a standard computer machine due to the combinatorial growth in the $|\mathcal{V} \cup C|^2 \times |\mathcal{K}|$, $|\mathcal{P}| \times |\mathcal{R}|$ and $|\mathcal{K}| \times |C|$ binary variables. Shuttle travel times between all pairs of vertices $i, j \in \mathcal{V} \cup C$ are provided in the 29×29 origin-destination (O-D) travel-time matrix shown in Table C.15 in Appendix C. The matrix is asymmetric, as travel distances are derived from the real road network extracted from OpenStreetMap. In this table, vertices #0 and #21 represent the two copies of Larissa station, while $\mathcal{O}_1$ and $\mathcal{O}_2$ correspond to Dekelia and Piraeus stations, respectively.

Request times and passenger demand for each pickup vertex $i \in \mathcal{P}$ are reported in Table 10. Requests span the operating period from 7:10 a.m. to 11:30 p.m. The rail service comprises $|\mathcal{R}| = 7$ scheduled departures on the Athens–Thessaloniki railway corridor during the operating day (Table 11), with the first departure at 7:18 a.m. and the last at 11:55 p.m.

As outlined in Section 3.2, we ran the extended network model multiple times while varying the ϵ-constant parameter, which imposes an upper bound on the number of shuttle buses available in the network. We solved nine instances with $\epsilon \in \{12, \dots, 20\}$,

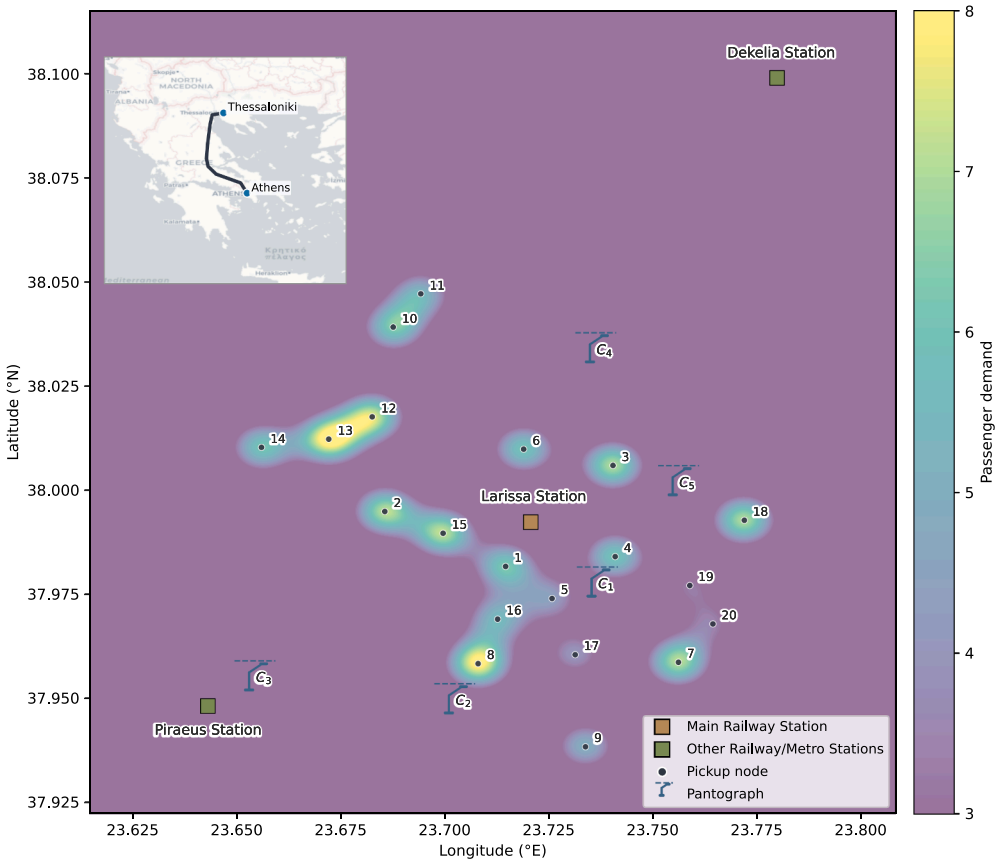

Fig. 4. Athens case study — Spatial layout of the main railway station (Larissa station), the two additional shuttle origin points (Dekelia and Piraeus stations), opportunity-charging pantographs, and pickup points, with passenger demand heat-mapped across the Athens metropolitan area. The upper-right inset illustrates the Athens–Thessaloniki rail corridor.

Table 11
Scheduled railway trip times y_r for the Athens–Thessaloniki railway line (minutes past midnight).

r	1	2	3	4	5	6	7
y	438	500	618	858	976	1098	1435

starting at the minimum fleet size that yields feasibility (12 vehicles) and increasing in unit steps to 20. Exploring fleets larger than the number of pickup points was deemed unnecessary. Across runs, the on-demand shuttles are routed to provide the most efficient passenger service, and the resulting set of solutions forms a Pareto set with respect to fleet size.

Table 12 summarizes, for each model run, the best objective value—total door-to-rail passenger travel time across all 20 pickup points—and the incremental improvement relative to the previous case. As ϵ increases, marginal gains diminish, reflecting the trade-off between fleet size and passenger travel time. Solutions up to case #5 ($\epsilon = 16$) are Pareto-optimal, after which the objective value plateaus at 615.83 minutes. Therefore, adding more than 16 on-demand shuttles yields no further reduction in passenger travel time.

The results in Table 12 are further illustrated through the approximated Pareto front in Fig. 5, which plots total door-to-rail passenger travel time f_1 against the number of available on-demand shuttle buses f_2 (equivalent to the ϵ value). Increasing the fleet from $\epsilon = 12$ to $\epsilon = 16$ reduces f_1 from 1455.16 to 615.83 minutes (839.33 minutes overall, corresponding to an average reduction of 7.17 minutes per passenger). Marginal improvements decrease with each additional shuttle, from 284.51 minutes ($12 \rightarrow 13$) and 250.72 minutes ($13 \rightarrow 14$) to 236 minutes ($14 \rightarrow 15$) and 68.11 minutes ($15 \rightarrow 16$), indicating substantial benefits up to 15 shuttles, followed by diminishing returns beyond $\epsilon = 16$. Notably, by $f_2 = 15$, the system achieves approximately 92% of the total travel-time reduction observed within the examined fleet-size range (12–16 shuttles).

Figs. C.10 – C.14 in Appendix C illustrate the five Pareto-optimal solutions for the extended Athens network, showing shuttle assignments to pickup demand and the resulting route trajectories. Opportunity charging occurs primarily at C_1 and C_5, the two charging sites closest to Larissa station, enabling vehicles to recharge shortly before route termination and thereby minimizing post-charge energy consumption. In several tours, vehicles cannot feasibly return to the railway station after serving pickup nodes without recharging, as doing so would violate the intermediate SOC threshold SOC_k^{up}. Since charging is permitted only when arrival SOC lies

Table 12
Model results across fleet sizes - Maximum electric on-demand shuttle fleet (ϵ-value), optimal objective (minutes), and percentage reduction between consecutive cases.

Case	ϵ-Constant Value	Best Objective Value	Decline Rate
1	12	1455.16	19.55%
2	13	1170.65	
3	14	919.93	21.42%
4	15	683.93	25.65%
5	16	615.83	9.96%
6	17	615.83	0.00%
7	18	615.83	0.00%
8	19	615.83	0.00%
9	20	615.83	0.00%

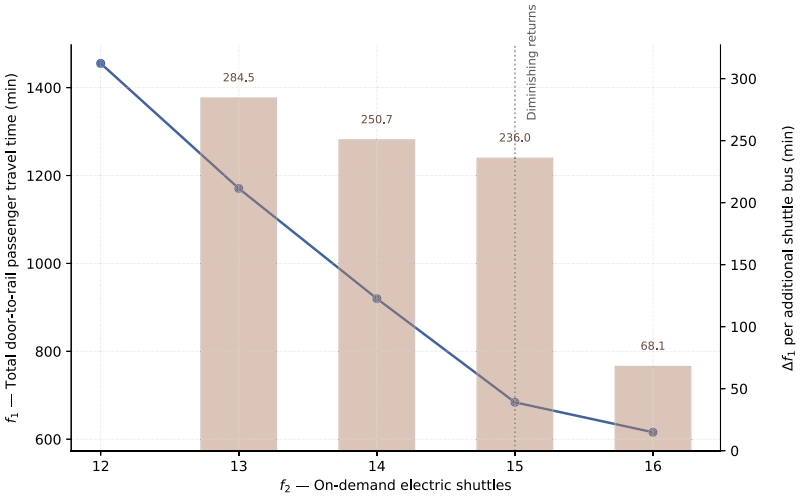

Fig. 5. Approximated pareto front of the EVRP–PTR, obtained with the ϵ-constraint method—f_1: total door-to-rail passenger travel time (minutes); f_2: number of electric on-demand shuttles—together with the corresponding Δf_1 per additional shuttle bus.

within the admissible range $[SOC_k^{\min}, SOC_k^{up}]$ (constraints (23)), shuttle routes and charging decisions are coordinated to maintain feasible battery levels upon charger arrival. The proximity of C_1 and C_5 to Larissa station explains their more frequent use relative to the remaining charging sites.

As shown in Fig. 5, and consistent with the decline rates reported in Table 12, reducing the available on-demand fleet leads to a sharp increase in total door-to-rail passenger travel time. With fewer electric shuttles serving the same demand ($|\mathcal{P}| = 20$ pickup nodes and 117 passengers), vehicles are assigned longer tours, increasing the likelihood of detours to opportunity chargers. These detours delay arrivals at Larissa station, causing some passengers to miss their most suitable rail departures (even after rescheduling) and incur higher platform waiting times w_i, thereby increasing f_1.

This mechanism is evident when comparing $\epsilon = 12$ and $\epsilon = 13$ (Figs. C.10 – C.11). Under $\epsilon = 12$, some shuttle tours combine multiple pickup nodes and require charging detours to satisfy SOC constraints, whereas under $\epsilon = 13$ additional vehicles allow more direct assignments. For example, pickup point $i = 2$ is served by a dedicated shuttle under $\epsilon = 13$, while under $\epsilon = 12$ it is grouped with $i = 14$, requiring a detour to C_1. These assignment differences lead to substantially higher rail-platform waiting times, increasing travel time by 108.71 minutes for passengers at $i = 14$ and 104.04 minutes for $i = 2$ under $\epsilon = 12$. A similar effect occurs at $i = 15$, where grouping with pickup node $i = 1$ under $\epsilon = 12$ causes passengers to miss the nearest rail departure and incur an additional 43.89 minutes of waiting. Such delays explain the observed increments in Δf_1 as fleet size decreases.

Table 13 illustrates how charging activity varies with fleet size (ϵ): as the number of available shuttles decreases, opportunity-charging events become more frequent. For each Pareto-optimal solution, the table reports the total number of charging events and the percentage of vehicles charging at least once. Notably, when $\epsilon = 16$, no vehicle requires charging, indicating that a sufficiently large fleet can operate without intermediate recharging. This reveals a secondary, cost-relevant trade-off: larger fleets reduce—or eliminate—charging interventions, whereas smaller fleets rely more on en-route charging to maintain comparable passenger service.

5.4.1. Computational performance analysis

Table 14 summarizes the Gurobi results for the nine problem instances, reporting the number of constraints (CNS), variables (VAR), explored nodes (NE), simplex iterations (SI), computational time in minutes (CT), and final optimality gap (OG). As shown, computational difficulty increases substantially as the available fleet size decreases. The most demanding instances correspond to

Table 13
Opportunity-charging activity by Pareto-optimal configuration: charging events and fleet participation rate (%).

Case	ϵ-Constant Value	Charging events	Charging rate
1	12	4	3.33%
2	13	3	23.08%
3	14	3	21.43%
4	15	2	13.33%
5	16	0	0.00%

Table 14
Results for the nine problem instances. CNS: constraints, VAR: variables, NE: nodes evaluated, SI: simplex iterations, CT: computation time (minutes), OG: optimality gap.

Case	ϵ-Constant Value	CNS	VAR	NE	SI	CT	OG
1	12	308,388	15,426	64,950	17,705,957	91.97	0.00%
2	13	355,850	16,875	40,509	12,165,306	1053.12	27.85%
3	14	406,712	18,364	1,100,492	283,188,304	6511.71	4.97%
4	15	460,974	19,893	131,832	4,347,470	31.87	0.00%
5	16	518,636	21,462	1,026,187	2,049,261	20.82	0.00%
6	17	579,698	23,071	1,326,962	1,534,164	37.60	0.00%
7	18	644,160	24,720	1,525,194	2,006,651	43.16	0.00%
8	19	712,022	26,409	1,087,524	1,931,283	40.19	0.00%
9	20	783,284	28,138	1,630,817	2,245,841	43.66	0.00%

cases #1 – #3 ($\epsilon \in \{12, 13, 14\}$), with computational time increasing by approximately 204 times between instances #4 ($\epsilon = 15$) and #3 ($\epsilon = 14$). For the two hardest instances (#2 – #3), the search was terminated after the optimality gap stopped improving. Across all instances, feasible solutions satisfying the constraints of Section 3 were obtained, including route feasibility, service-time ordering, railway timetable rescheduling, SOC requirements, and charger-capacity restrictions. No charger-occupancy conflicts were observed, confirming the validity of the charging-sequence formulation. Overall, the model consistently served all pickup locations ($|\mathcal{P}| = 20$) and accommodated 117 passengers across the examined fleet sizes.

5.4.2. *Public transport rescheduling sensitivity analysis*

In this subsection, a sensitivity analysis of the Public Transport Rescheduling (PTR) component is conducted for the Athens case study. Two additional scenarios are examined, with railway timetable deviations of $s = 0$ and $s = 1$ minute, and compared with the main case study ($s = 2$ minutes). The objective is to assess the impact of railway timetable flexibility on passenger door-to-rail travel time. This analysis is particularly relevant for the Athens–Thessaloniki railway corridor, a long-distance service with relatively infrequent departures, where timetable adjustments may influence passenger experience more strongly than in high-frequency urban PT systems.

Fig. 6 presents the corresponding Pareto fronts, illustrating the trade-off between total door-to-rail passenger travel time (f_1) and the number of available on-demand shuttle buses (f_2) under different values of the railway timetable deviation parameter s. The accompanying bar plots report objective differences (Δf_1) relative to the case $s = 2$ minutes. All differences are positive, indicating that reducing railway timetable flexibility increases passenger travel time. The $s = 2$ minutes configuration consistently achieves the lowest travel times, followed by $s = 1$ minute, while $s = 0$ performs the worst. All Pareto fronts begin at $\epsilon = 12$ vehicles and do not offer additional non-dominated solutions after $\epsilon = 16$. The observed values of Δf_1 highlight the benefits of timetable flexibility. Compared with $s = 2$ minutes, travel-time differences range from approximately 330–400 minutes for the $s = 1$ minute case and 355–420 minutes for $s = 0$, demonstrating that even small timetable adjustments (±1-2 minutes) can substantially improve passenger service quality. In general, these differences increase with on-demand fleet size. The largest relative gap between the cases of $s = 1$ minute and $s = 2$ minutes (17.61%) occurs at $\epsilon : 15 \rightarrow 16$, whereas for $s = 0$ and $s = 2$, the maximum gap (11.35%) occurs at $\epsilon : 12 \rightarrow 13$. Overall, the results indicate that even limited timetable flexibility substantially improves coordination between on-demand and railway services, particularly when fleet resources are constrained.

5.4.3. *Baseline scenario analysis*

The proposed EVRP–PTR framework incorporates two key components: (i) timetable coordination between on-demand and railway services, and (ii) opportunity charging for the electric shuttle fleet. To evaluate the benefits of this integrated framework, the main Athens case study is compared with a baseline scenario in which both components are disabled. The resulting Pareto fronts and corresponding objective differences (Δf_1) are presented in Fig. 7.

As shown, the baseline Pareto front exhibits limited variability, beginning at $\epsilon = 13$ vehicles and saturating at $\epsilon = 14$, whereas the integrated framework initiates at a smaller fleet size ($\epsilon = 12$) and continues improving up to $\epsilon = 16$. Consequently, the integrated framework provides greater flexibility in fleet-size decisions while consistently achieving lower passenger door-to-rail travel times. The objective differences Δf_1 further highlight this advantage. With the exception of $\epsilon = 13$, where the baseline scenario performs

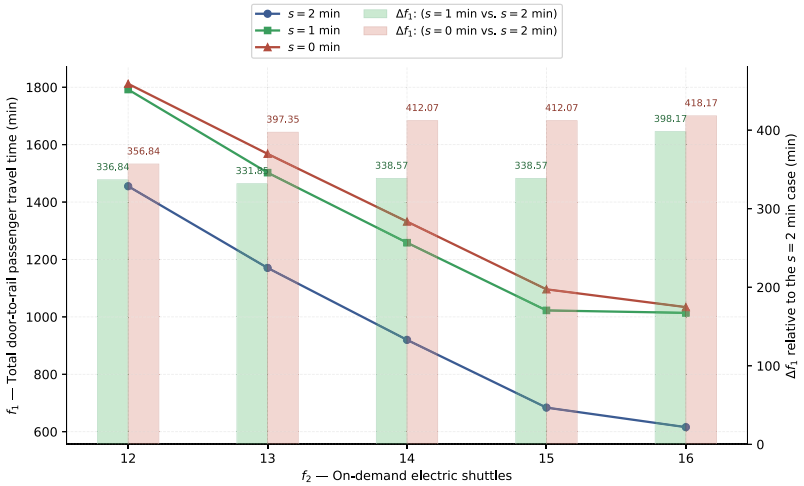

Fig. 6. Approximated pareto fronts of the EVRP–PTR under three railway timetable deviation settings—(i) $s = 0$, (ii) $s = 1$ min, and (iii) $s = 2$ min obtained using the ϵ-Constraint Method, together with the corresponding Δf_1 relative to the main Athens case study ($s = 2$ min); f_1: total door-to-rail passenger travel time (minutes); f_2: number of electric on-demand shuttles.

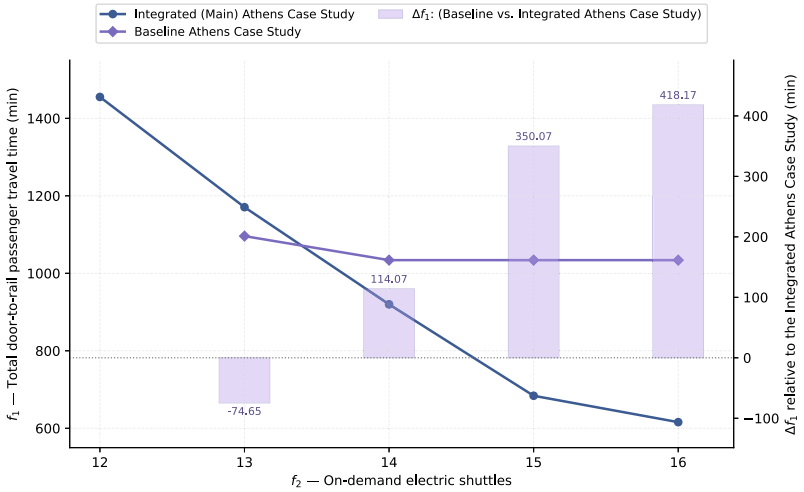

Fig. 7. Approximated Pareto fronts of the EVRP–PTR for the integrated Athens case study and the baseline scenario, obtained using the ϵ-Constraint Method, together with the corresponding Δf_1 relative to the integrated case; f_1: total door-to-rail passenger travel time (minutes); f_2: number of electric on-demand shuttles.

better by 74.65 minutes, the integrated framework outperforms the baseline by approximately 114–418 minutes. These improvements mainly arise from reduced passenger waiting times at the railway station due to better synchronization between shuttle arrivals and railway departures. The isolated superior performance of the baseline at $\epsilon = 13$ appears incidental, reflecting a favorable demand-fleet alignment without requiring timetable coordination or charging interventions. Overall, the results demonstrate that integrating timetable coordination and opportunity charging within the EVRP–PTR framework substantially improves system performance and enables more effective use of additional shuttle vehicles to reduce passenger travel times.

5.4.4. Modeling travel-time uncertainties with stochastic and chance constraint approaches

To account for travel-time uncertainty in the Athens case study, travel-time scenarios ($|S|$) are generated for each feasible arc $(i, j) \in \mathcal{A}$, yielding scenario-dependent travel times $t_{s,ij}$. These realizations are incorporated into the EVRP–PTR framework under two probability settings, $\xi = 90\%$ and $\xi = 100\%$, enforcing constraints (B.3), (B.6), (B.9), (B.13), (B.16), and (B.20) to hold in at least 90% or 100% of scenarios, respectively. All scenarios are generated from the same log-normal distribution of shuttle travel times.

Fig. 8 compares the deterministic Pareto front (corresponding to the main Athens case study) with those obtained under stochastic ($\xi = 100\%$) and chance-constrained ($\xi = 90\%$) settings. In both uncertainty-based approaches, Pareto fronts shift upward, indicating consistently higher total door-to-rail passenger travel times relative to the deterministic case. Under the stochastic approach, additional passenger delays range from approximately 612 minutes at $\epsilon = 14$ to 624–629 minutes for larger fleets. Under the chance-

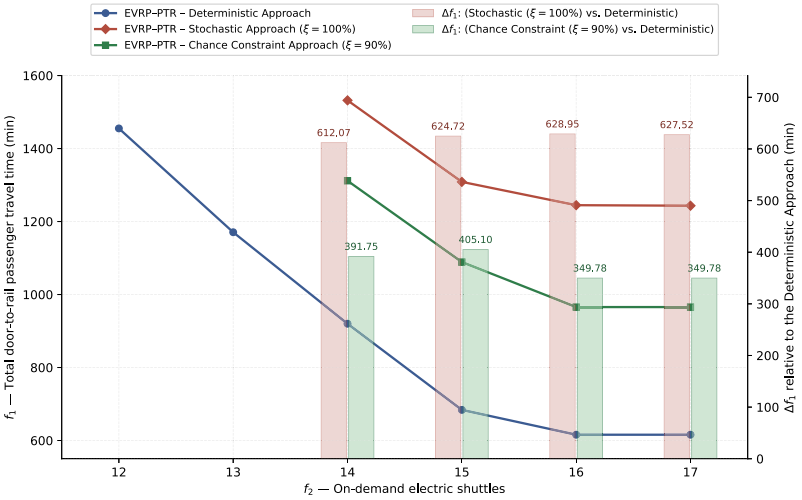

Fig. 8. Approximated pareto fronts of the EVRP–PTR under deterministic, stochastic ($\xi = 100\%$), and chance-constrained ($\xi = 90\%$) settings, obtained using the ϵ-Constraint Method, together with the corresponding Δf_1 relative to the deterministic case; f_1: total door-to-rail passenger travel time (minutes); f_2: number of electric on-demand shuttles.

constrained approach, increases are smaller (approximately 350–405 minutes), yielding a Pareto front between the stochastic and deterministic cases. These increases are primarily driven by longer passenger waiting times at the railway station (w_i).

Travel-time uncertainty also reduces the feasible Pareto region. While the deterministic model yields feasible solutions from $\epsilon = 12$, both uncertainty-based approaches are infeasible for $\epsilon \in \{12, 13\}$, requiring larger fleets to maintain reliable service. Pareto-front saturation occurs at $\epsilon = 16$ for $\xi = 90\%$ and $\epsilon = 17$ for $\xi = 100\%$, compared with $\epsilon = 16$ in the deterministic case, while the total travel-time reduction across the Pareto range decreases substantially (346.07 minutes for $\xi = 90\%$ and 288.65 minutes for $\xi = 100\%$, compared with 839.33 minutes in the deterministic case). Interestingly, charging activity is lower under uncertainty: only one charging event occurs across the Pareto-optimal solutions for both ξ-settings ($\epsilon = 14$, pantograph C_1), compared with five charging events in the deterministic case over the corresponding Pareto range $\epsilon \in \{14, 15, 16\}$ (see Table 13). This occurs because the model prioritizes passenger travel-time minimization by avoiding intermediate charging whenever feasible, subject to SOC constraints. Overall, travel-time uncertainty leads to narrower Pareto-optimal regions and highlights a trade-off between system robustness and passenger service performance.

5.4.5. *Multi-origin athens case study*

This subsection evaluates the applicability of the proposed EVRP–PTR framework under a multi-origin shuttle configuration, where shuttles can start their trips from multiple depots. Unlike the main Athens case study, where all electric shuttles depart from Larissa station (the main railway hub), this scenario allows shuttle buses to initiate their routes from two additional origin points (depots): Dekelia station ($\mathcal{O}_1$) and Piraeus station ($\mathcal{O}_2$). All remaining network parameters are kept unchanged, and the locations of these additional origin points are shown in Fig. 4.

As in the main single-origin shuttle Athens case study, the model is solved iteratively for different ϵ-values. For each experiment, the number of available shuttles at Larissa, Dekelia, and Piraeus stations is predefined, with the largest share assigned to Larissa Station due to its role as the primary railway hub. Fig. 9 compares the Pareto fronts of the single-origin and multi-origin shuttle Athens case studies. In both cases, at least $\epsilon = 12$ shuttles are required, while improvements in total door-to-rail passenger travel time stop at $\epsilon = 16$, after which additional vehicles lead to dominated solutions.

However, the multi-origin configuration consistently achieves lower passenger door-to-rail travel times than the single-origin case for $\epsilon \in \{12, 13, 14, 15\}$. The largest improvement is observed at $\epsilon = 12$, where the total passenger travel time is reduced by 241.70 minutes. This benefit can be attributed to the spatial distribution of the new shuttle origins, which improves coverage of peripheral and outlier pickup points compared with the single-origin configuration. As fleet size increases, the advantage gradually diminishes, and for $\epsilon = 16$ the two configurations yield nearly identical results, with a negligible difference of 0.03 minutes. This indicates that when a sufficiently large on-demand fleet is available, the single-origin configuration can also provide adequate spatial coverage, reducing the marginal benefit of additional shuttle origin points.

Regarding charging behavior, shuttles initiating from the additional origin points are primarily used to serve nearby pickup nodes while preserving battery feasibility. Unlike the main Athens case study, the number of charging events does not decrease monotonically as ϵ increases, mainly due to the spatial location of Dekelia and Piraeus stations, which alters routing and charging patterns. As in the main case study, pantographs C_1 and C_5 are most frequently utilized, while charger C_4 is additionally used, primarily by shuttles originating from Dekelia Station. Overall, these results confirm the applicability of the EVRP–PTR framework to multi-origin shuttle operations while satisfying passenger service, routing, charging, and vehicle operating constraints.

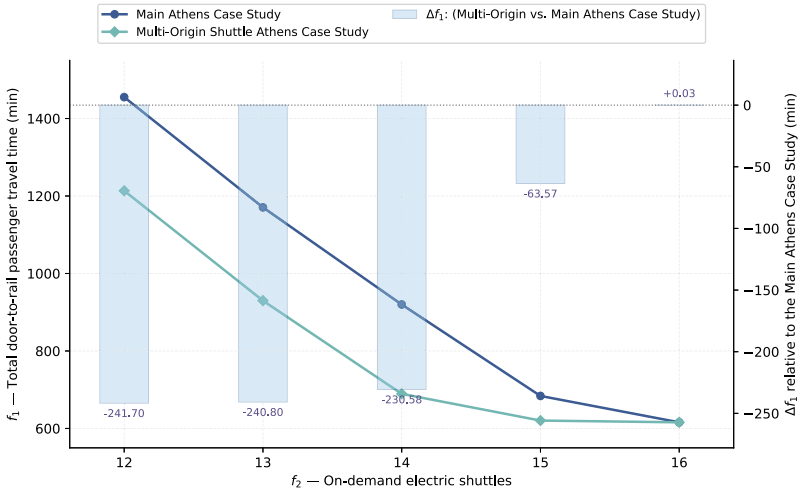

Fig. 9. Approximated pareto fronts of the EVRP–PTR for the multi-origin shuttle and main Athens case studies, obtained using the ϵ-Constraint Method, together with the corresponding Δf_1 relative to the main Athens case study; f_1: total door-to-rail passenger travel time (minutes); f_2: number of electric on-demand shuttles.

Concluding remarks

The present study proposed a multi-objective optimization framework for the Electric Vehicle Routing and Public Transport Rescheduling Problem (EVRP–PTR), coordinating an electric demand-responsive shuttle feeder service with railway operations. The proposed EVRP–PTR was reformulated as a mixed-integer linear programming (MILP) model integrating routing, temporal synchronization, state-of-charge (SOC), opportunity charging, and public transport (PT) rescheduling constraints. To better reflect real-world operations, the framework was further extended to account for travel-time uncertainty through stochastic and chance-constrained formulations.

The proposed EVRP–PTR model was evaluated on both a toy network and a real Athens case study involving 20 pickup points, up to 20 electric shuttle buses, five pantographs, and seven railway trips along the Athens–Thessaloniki railway corridor. Using the ϵ-constraint method, the resulting Pareto front showed that the examined demand can be effectively served by an on-demand fleet of $\epsilon \in \{12, 13, 14, 15, 16\}$ vehicles, while reducing total passenger door-to-rail travel time by approximately 840 minutes across the Pareto front. Moreover, increasing fleet size eliminated the need for intermediate en-route charging. When considering travel-time uncertainty, Pareto fronts shifted upward and feasible Pareto regions narrowed, indicating the need for a minimum fleet size of $\epsilon = 14$ vehicles to maintain comparable service quality.

The analyses further demonstrated the importance of the Public Transport Rescheduling (PTR) component, showing that even limited PT timetable flexibility can substantially improve synchronization between on-demand and railway services, thereby enhancing passenger service quality. In addition, the EVRP–PTR framework proved computationally tractable for mid-sized networks and applicable to multi-depot shuttle operations, demonstrating its ability to generalize to networks with different shuttle starting locations.

Future research may explore several directions for extending the proposed EVRP–PTR framework. First, the model could be applied to PT systems with more flexible timetables, such as metro, tram, and high-frequency bus services, where broader rescheduling windows are feasible compared with long-distance railway operations. From a methodological perspective, dynamic routing and rolling-horizon optimization could enable electric shuttle buses to continuously adapt their routes in response to evolving passenger demand and operational disturbances in real time. In addition, incorporating charging-price variability into the model may enable the investigation of trade-offs among passenger door-to-PT travel time, fleet size, and charging operation costs, providing additional planning insights for operators and decision-makers. Finally, the development of problem-specific heuristic and metaheuristic solution approaches could support the computation of high-quality solutions for larger-scale problem instances, enhancing the applicability of the proposed framework to more complex real-world settings.

Disclosure statement

There is no conflict of interest. Given Dr. Konstantinos Gkiotsalitis and Prof. Oded Cats role as members of the Editorial Board for Transportation Research Part C, they had no involvement in the peer review of this article and had no access to information regarding its peer review. Full responsibility for the editorial process for this article was delegated to another journal editor.

CRediT authorship contribution statement

Androniki Dimitriadou: Writing – original draft, Visualization, Validation, Software, Methodology, Investigation, Data curation, Conceptualization; **Konstantinos Gkiotsalitis:** Writing – review & editing, Supervision, Methodology, Conceptualization; **Tao Liu:** Writing – review & editing, Methodology; **Oded Cats:** Writing – review & editing, Methodology.

Data availability

Data will be made available on request.

Acknowledgement

The present work is funded by the PT-MaaS Project (Scheduling Integration of Public Transport and Shared Mobility - Project Number: 015073). This project is carried out within the framework of the National Recovery and Resilience Plan Greece 2.0, funded by the European Union – NextGenerationEU (Implementation body: HFRI).

Appendix A.

Lemma 1. *Constraints (16):* $u_o^k = u_i^k - t_{oi} \mid x_{oi}^k = 1 \;\; \forall o \in \mathcal{O} \setminus \{p+1\}, \forall i \in \mathcal{P}, \forall k \in \mathcal{K}$ *and the following set of constraints are equisatisfiable:*

$$u_o^k \geq u_i^k - t_{oi} - M(1 - x_{oi}^k) \qquad \forall o \in \mathcal{O} \setminus \{p+1\}, \forall i \in \mathcal{P}, \forall k \in \mathcal{K} \tag{A.1}$$

$$u_o^k \leq u_i^k - t_{oi} + M(1 - x_{oi}^k) \qquad \forall o \in \mathcal{O} \setminus \{p+1\}, \forall i \in \mathcal{P}, \forall k \in \mathcal{K} \tag{A.2}$$

Proof. The equality condition $u_o^k = u_i^k - t_{oi}$ in the logical expression of constraints (16) is enforced through constraints (A.1) and (A.2), conditional on the binary variable x_{oi}^k being equal to 1. Specifically, these constraints ensure that $u_o^k = u_i^k - t_{oi}$ whenever $x_{oi}^k = 1$. Otherwise, the departure time of shuttle bus $k \in \mathcal{K}$ from its starting point, u_o^k, is allowed to take any value within the interval [$-M$, M]. □

Similar to constraints (16), constraints (23), (26), (28a), (37), (41), and (43) are nonlinear due to embedded logical expressions. With the exception of constraints (26), which are linearized separately because of their more complex nonlinear structure, the remaining constraints are linearized following the same approach as constraints (16). This process results in the ten auxiliary constraints presented in (A.3) – (A.12).

$$SOC_k^j \geq SOC_k^{\min} - M(1 - \delta_{kj}) \qquad \forall j \in C, \forall k \in \mathcal{K} \tag{A.3}$$

$$SOC_k^j \leq SOC_k^{up} + M(1 - \delta_{kj}) \qquad \forall j \in C, \forall k \in \mathcal{K} \tag{A.4}$$

$$g_j^k \geq u_i^k + \beta q_i \theta_i^k + t_{ij} - M(1 - x_{ij}^k) \qquad \forall (i,j) \in \mathcal{A} : j \in \mathcal{V}, \forall k \in \mathcal{K} \tag{A.5}$$

$$g_j^k \leq u_i^k + \beta q_i \theta_i^k + t_{ij} + M(1 - x_{ij}^k) \qquad \forall (i,j) \in \mathcal{A} : j \in \mathcal{V}, \forall k \in \mathcal{K} \tag{A.6}$$

$$b_i \geq \tau_k + \alpha - M(1 - \theta_i^k) \qquad \forall i \in \mathcal{P}, \forall k \in \mathcal{K} \tag{A.7}$$

$$b_i \leq \tau_k + \alpha + M(1 - \theta_i^k) \qquad \forall i \in \mathcal{P}, \forall k \in \mathcal{K} \tag{A.8}$$

$$h_r \geq -s - M(1 - l_{ir}) \qquad \forall i \in \mathcal{P}, \forall r \in \mathcal{R} \tag{A.9}$$

$$h_r \leq s + M(1 - l_{ir}) \qquad \forall i \in \mathcal{P}, \forall r \in \mathcal{R} \tag{A.10}$$

$$w_i \geq (y_r + h_r) - b_i - M(1 - l_{ir}) \qquad \forall i \in \mathcal{P}, \forall r \in \mathcal{R} \tag{A.11}$$

$$w_i \leq (y_r + h_r) - b_i + M(1 - l_{ir}) \qquad \forall i \in \mathcal{P}, \forall r \in \mathcal{R} \tag{A.12}$$

Constraints (21) are nonlinear due to the multiplication between the departure state-of-charge variable $\overline{SOC_k^i}$ and the binary routing variable x_{ij}^k. We linearize this term through constraints (A.13) and (A.14). Under this reformulation, whenever shuttle bus $k \in \mathcal{K}$ traverses arc $(i,j) \in \mathcal{A}$, i.e., $x_{ij}^k = 1$, the arrival state-of-charge at node $j \in \mathcal{V} \cup C$, SOC_k^j, is enforced to equal the departure state-of-charge from node i, $\overline{SOC_k^i}$, reduced by the energy consumption along arc (i,j), namely γd_{ij}. Conversely, when $x_{ij}^k = 0$, the value of SOC_k^j is relaxed and bounded only through the imposed big-M limits.

$$SOC_k^j \geq \overline{SOC_k^i} - \gamma d_{ij} - M(1 - x_{ij}^k) \qquad \forall (i,j) \in \mathcal{A} : j \in \mathcal{V} \cup C, \forall k \in \mathcal{K} \tag{A.13}$$

$$SOC_k^j \leq \overline{SOC_k^i} - \gamma d_{ij} + M(1 - x_{ij}^k) \qquad \forall (i,j) \in \mathcal{A} : j \in \mathcal{V} \cup C, \forall k \in \mathcal{K} \tag{A.14}$$

In constraints (24), nonlinearity arises from bilinear products involving the routing and charging decision variables x_{ij}^k and δ_{kj}, together with the time and assignment variables u_i^k and θ_i^k. Similarly, constraints (25) include the bilinear term $f_{kj}\delta_{kj}$, while constraints (42) involve the product $h_r l_{ir}$ on the left-hand side of the inequality. Since these terms exhibit the same bilinear structure as

the nonlinear term in constraints (21), they are linearized using an analogous reformulation approach, resulting in the five auxiliary linear constraints presented in (A.15) – (A.19).

$$f_{kj} + M(1-\delta_{kj}) \geq u_i^k + \beta q_i \theta_i^k + t_{ij} - M(1-x_{ij}^k) \qquad \forall (i,j) \in \mathcal{A} : j \in C, \forall k \in \mathcal{K} \tag{A.15}$$

$$f_{kj} - M(1-\delta_{kj}) \leq u_i^k + \beta q_i \theta_i^k + t_{ij} + M(1-x_{ij}^k) \qquad \forall (i,j) \in \mathcal{A} : j \in C, \forall k \in \mathcal{K} \tag{A.16}$$

$$\lambda_{kj} \geq f_{kj} + \rho - M(1-\delta_{kj}) \qquad \forall j \in C, \forall k \in \mathcal{K} \tag{A.17}$$

$$\lambda_{kj} \leq f_{kj} + \rho + M(1-\delta_{kj}) \qquad \forall j \in C, \forall k \in \mathcal{K} \tag{A.18}$$

$$(y_r + h_r) + M(1-l_{ir}) \geq b_i \qquad \forall i \in \mathcal{P}, \forall r \in \mathcal{R} \tag{A.19}$$

Finally, constraints (26) are non-convex due to the embedded logical conditions governing charger occupancy. To address this nonlinearity, constraints (26) are reformulated into three distinct components through constraints (A.20) – (A.25), introducing the auxiliary binary variables $\sigma_{k\phi j}$, $\iota_{k\phi j}$, and $\mu_{k\phi j}$, together with a very small positive constant ζ.

Lemma 2. *Constraints (26): $\delta_{\phi j} + \delta_{kj} \leq 1$ if $f_{\phi j} \leq f_{kj} \wedge f_{kj} < \lambda_{\phi j} \forall k \in \mathcal{K}, \forall \phi \in \mathcal{K} \setminus \{k\}, \forall j \in C$ and the following set of constraints are equisatisfiable:*

$$f_{\phi j} \leq f_{kj} + M(1-\sigma_{k\phi j}) \qquad \forall k \in \mathcal{K}, \forall \phi \in \mathcal{K} \setminus \{k\}, \forall j \in C \tag{A.20}$$

$$f_{\phi j} \geq f_{kj} + \zeta - M\sigma_{k\phi j} \qquad \forall k \in \mathcal{K}, \forall \phi \in \mathcal{K} \setminus \{k\}, \forall j \in C \tag{A.21}$$

$$f_{kj} \leq \lambda_{\phi j} - \zeta + M(1-\iota_{k\phi j}) \qquad \forall k \in \mathcal{K}, \forall \phi \in \mathcal{K} \setminus \{k\}, \forall j \in C \tag{A.22}$$

$$f_{kj} \geq \lambda_{\phi j} - M\iota_{k\phi j} \qquad \forall k \in \mathcal{K}, \forall \phi \in \mathcal{K} \setminus \{k\}, \forall j \in C \tag{A.23}$$

$$\mu_{k\phi j} = \min(\sigma_{k\phi j}, \iota_{k\phi j}) \qquad \forall k \in \mathcal{K}, \forall \phi \in \mathcal{K} \setminus \{k\}, \forall j \in C \tag{A.24}$$

$$\delta_{\phi j} + \delta_{kj} \leq 1 + M(1-\mu_{k\phi j}) \qquad \forall k \in \mathcal{K}, \forall \phi \in \mathcal{K} \setminus \{k\}, \forall j \in C \tag{A.25}$$

Proof. The first inequality condition, $f_{\phi j} \leq f_{kj}$, in the logical expression of constraints (26) is reformulated through constraints (A.20) – (A.21). These constraints ensure that the binary variable $\sigma_{k\phi j}$ equals 1 whenever shuttle bus $k \in \mathcal{K}$ initiates charging at charger $j \in C$ no earlier than shuttle bus $\phi \in \mathcal{K} \setminus \{k\}$, i.e., when $f_{\phi j} \leq f_{kj}$, and 0 otherwise. The small positive constant ζ is introduced in constraints (A.21) to reformulate the strict inequality (>) into an equivalent non-strict form (≥). Similarly, the second inequality condition, $f_{kj} < \lambda_{\phi j}$, is reformulated through constraints (A.22) – (A.23). These constraints ensure that the binary variable $\iota_{k\phi j}$ equals 1 whenever shuttle bus k initiates charging before shuttle bus ϕ completes charging at charger j, and 0 otherwise. Again, the small positive constant ζ is used to represent the strict inequality (<) in a linear form. The third logical condition of constraints (26), expressed as $\delta_{\phi j} + \delta_{kj} \leq 1$, is reformulated through constraints (A.24) – (A.25). Constraints (A.24) define the binary variable $\mu_{k\phi j}$ as the minimum of $\sigma_{k\phi j}$ and $\iota_{k\phi j}$. Consequently, when $\mu_{k\phi j} = 1$, the charging intervals of shuttle buses k and ϕ overlap, and constraints (A.25) prohibit both vehicles from being assigned to the same charger j. Otherwise, $\mu_{k\phi j} = 0$. □

From the linearization of constraints (26), the constraints (A.24) present nonlinearity. To address this, we introduce an additional binary variable $\psi_{k\phi j}$ to replace the nonlinear constraints (A.24) with the following linear (A.26) – (A.29). Note that constraints (A.24) and (A.26) – (A.29) are equisatisfiable.

$$\mu_{k\phi j} \leq \sigma_{k\phi j} \qquad \forall k \in \mathcal{K}, \forall \phi \in \mathcal{K} \setminus \{k\}, \forall j \in C \tag{A.26}$$

$$\mu_{k\phi j} \leq \iota_{k\phi j} \qquad \forall k \in \mathcal{K}, \forall \phi \in \mathcal{K} \setminus \{k\}, \forall j \in C \tag{A.27}$$

$$\mu_{k\phi j} \geq \sigma_{k\phi j} - M\psi_{k\phi j} \qquad \forall k \in \mathcal{K}, \forall \phi \in \mathcal{K} \setminus \{k\}, \forall j \in C \tag{A.28}$$

$$\mu_{k\phi j} \geq \iota_{k\phi j} + M(\psi_{k\phi j} - 1) \qquad \forall k \in \mathcal{K}, \forall \phi \in \mathcal{K} \setminus \{k\}, \forall j \in C \tag{A.29}$$

Appendix B.

$$C_{1,s,ik} \geq -M(1-c_{1,s,ik}) \qquad \forall i \in \mathcal{P}, \forall k \in \mathcal{K}, \forall s \in \{1,\ldots,S\} \tag{B.1}$$

$$C_{1,s,ik} \leq -\zeta + Mc_{1,s,ik} \qquad \forall i \in \mathcal{P}, \forall k \in \mathcal{K}, \forall s \in \{1,\ldots,S\} \tag{B.2}$$

$$\sum_{s \in S} c_{1,s,ik} \geq \xi |S| \sum_{j:(i,j) \in \mathcal{A}} x_{ij}^k \qquad \forall i \in \mathcal{P}, \forall k \in \mathcal{K} \tag{B.3}$$

$$C_{2,s,k\phi j} \leq M(1-c_{2,s,k\phi j}) \qquad \forall k \in \mathcal{K}, \forall \phi \in \mathcal{K} \setminus \{k\}, \forall j \in C, \forall s \in \{1,\ldots,S\} \tag{B.4}$$

$$C_{2,s,k\phi j} \geq \zeta - Mc_{2,s,k\phi j} \qquad \forall k \in \mathcal{K}, \forall \phi \in \mathcal{K} \setminus \{k\}, \forall j \in C, \forall s \in \{1,\ldots,S\} \tag{B.5}$$

$$\sum_{s \in S} c_{2,s,k\phi j} \geq \xi |S| \qquad \forall k \in \mathcal{K}, \forall \phi \in \mathcal{K} \setminus \{k\}, \forall j \in C \tag{B.6}$$

$$C_{3,s,i} \leq M(1-c_{3,s,i}) \qquad \forall i \in \mathcal{P}, \forall s \in \{1,\ldots,S\} \tag{B.7}$$

$$C_{3,s,i} \geq \zeta - Mc_{3,s,i} \qquad \forall i \in \mathcal{P}, \forall s \in \{1,\ldots,S\} \tag{B.8}$$

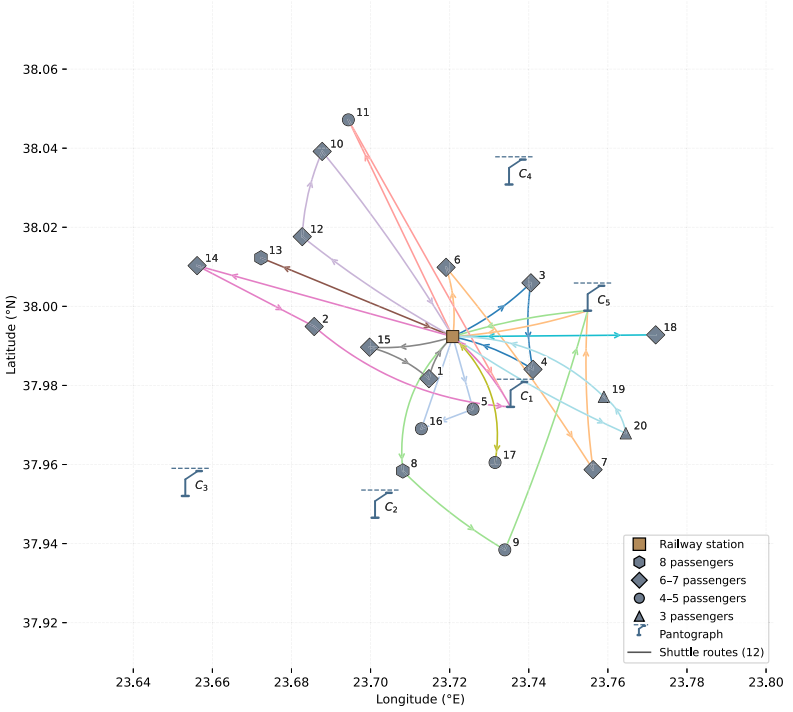

Fig. C.10. Travel route paths of the $\epsilon = 12$ electric shuttles (Deterministic Approach).

$$\sum_{s\in S} c_{3,s,i} \geq \xi|S| \qquad \forall i \in \mathcal{P} \tag{B.9}$$

$$C_{4,s,ko} \leq M(1 - c_{4,s,ko}) \qquad \forall o \in \mathcal{O} \setminus \{p+1\}, \forall k \in \mathcal{K}, \forall s \in \{1,\ldots,S\} \tag{B.10}$$

$$C_{4,s,ko} \geq \zeta - M c_{4,s,ko} \qquad \forall o \in \mathcal{O} \setminus \{p+1\}, \forall k \in \mathcal{K}, \forall s \in \{1,\ldots,S\} \tag{B.11}$$

$$c_{4,s,ko} \leq \sum_{i:(o,i)\in\mathcal{A}} x^k_{oi} \qquad \forall o \in \mathcal{O} \setminus \{p+1\}, \forall k \in \mathcal{K}, \forall s \in \{1,\ldots,S\} \tag{B.12}$$

$$\sum_{s\in S} c_{4,s,ko} \geq \xi|S| \sum_{i:(o,i)\in\mathcal{A}} x^k_{oi} \qquad \forall o \in \mathcal{O} \setminus \{p+1\}, \forall k \in \mathcal{K} \tag{B.13}$$

$$C_{5,s,i} \leq M(1 - c_{5,s,i}) \qquad \forall i \in \mathcal{P}, \forall s \in \{1,\ldots,S\} \tag{B.14}$$

$$C_{5,s,i} \geq \zeta - M c_{5,s,i} \qquad \forall i \in \mathcal{P}, \forall s \in \{1,\ldots,S\} \tag{B.15}$$

$$\sum_{s\in S} c_{5,s,i} \geq \xi|S| \qquad \forall i \in \mathcal{P} \tag{B.16}$$

$$C_{6,s,ir} \geq -M(1 - c_{6,s,ir}) \qquad \forall i \in \mathcal{P}, \forall r \in \mathcal{R}, \forall s \in \{1,\ldots,S\} \tag{B.17}$$

$$C_{6,s,ir} \leq -\zeta + M c_{6,s,ir} \qquad \forall i \in \mathcal{P}, \forall r \in \mathcal{R}, \forall s \in \{1,\ldots,S\} \tag{B.18}$$

$$c_{6,s,ir} \leq l_{ir} \qquad \forall i \in \mathcal{P}, \forall r \in \mathcal{R}, \forall s \in \{1,\ldots,S\} \tag{B.19}$$

$$\sum_{s\in S} c_{6,s,ir} \geq \xi|S| l_{ir} \qquad \forall i \in \mathcal{P}, \forall r \in \mathcal{R} \tag{B.20}$$

Constraints (B.3), (B.6), (B.9), (B.13), (B.16), and (B.20) count the number of scenarios in which the stochastic conditions are satisfied and compare this count against the threshold $\xi|S|$. In particular, $C_{1,s,ik}$ and $C_{6,s,ir}$ are required to be non-negative, whereas $C_{2,s,k\phi j}$, $C_{3,s,i}$, $C_{4,s,ko}$, and $C_{5,s,i}$ must be non-positive. As discussed in Section 4, the conditions $C_{1,s,ik} \geq 0$ and $C_{2,s,k\phi j} \leq 0$ must hold for all scenarios $s \in S$; therefore, $\xi = 1$ in these cases. In constraints (B.3), the term $\sum_{j:(i,j)\in\mathcal{A}} x^k_{ij}$ ensures that the condition is enforced only for assigned pickup-vehicle pairs (i,k), thereby avoiding unnecessary computations. A similar logic is applied to $c_{4,s,ko}$ through constraints (B.12)–(B.13), ensuring that it equals 1 only if shuttle bus $k \in \mathcal{K}$ serves at least one pickup vertex $i \in \mathcal{P}$ (i.e., $x^k_{oi} = 1$ for at least one i). Likewise, $c_{6,s,ir}$ is restricted to equal 1 only for pickup-railway trip pairs (i,r) with $l_{ir} = 1$, as enforced by constraints (B.19)–(B.20).

Appendix C.

Table C.15
Travel time t_{ij} from vertex $i \in \mathcal{V} \cup C$ to vertex $j \in \mathcal{V} \cup C$ (minutes) – Athens case study network.

O\D	0	$\mathcal{O}_1$	$\mathcal{O}_2$	1	2	3	4	5	6	7	8	9	10	11	12	13	14	15	16	17	18	19	20	21	C_1	C_2	C_3	C_4	C_5
0	$+\infty$	28.10	19.06	3.01	9.40	6.76	5.17	7.29	5.67	11.12	9.77	14.64	14.10	15.37	11.16	12.26	14.96	5.53	7.29	9.28	10.73	9.30	11.00	$+\infty$	5.48	13.52	16.61	10.46	7.85
$\mathcal{O}_1$	27.26	$+\infty$	44.47	30.27	30.65	24.31	30.81	33.14	25.05	36.97	36.66	40.49	23.79	21.57	28.61	31.13	34.23	30.92	34.03	35.13	29.88	33.17	36.58	27.26	31.33	40.24	42.11	17.84	27.51
$\mathcal{O}_2$	18.41	44.35	$+\infty$	15.68	14.27	23.99	20.71	20.99	20.80	22.97	13.57	18.78	24.49	26.61	19.26	18.07	17.60	15.99	14.52	17.92	27.23	23.34	24.33	18.41	19.82	11.40	2.20	27.23	24.60
1	3.26	30.41	16.88	$+\infty$	7.22	8.30	6.02	6.99	8.22	11.56	6.95	13.72	16.45	17.84	11.89	11.80	13.79	4.93	4.32	8.98	12.26	9.74	11.43	3.26	5.19	10.63	14.43	12.76	9.38
2	9.35	31.37	14.46	7.17	$+\infty$	12.60	12.67	13.82	7.82	18.38	12.35	19.39	11.54	13.66	6.31	5.60	8.13	4.60	10.28	15.35	18.91	16.57	18.26	9.35	12.01	15.63	12.69	14.25	15.17
3	6.08	24.09	24.63	9.08	12.77	$+\infty$	7.25	10.38	7.47	14.07	14.65	17.73	14.95	14.71	13.66	15.52	18.77	10.89	12.02	12.37	8.19	9.18	12.74	6.08	8.57	17.49	22.18	7.07	3.66
4	4.88	29.76	21.04	6.01	12.25	6.36	$+\infty$	5.68	9.51	8.61	10.70	13.01	17.94	19.22	14.89	15.83	18.39	8.96	8.44	7.65	7.66	5.88	8.48	4.88	3.79	12.79	18.59	12.41	5.38
5	5.92	32.93	19.89	4.85	11.09	10.28	5.28	$+\infty$	10.88	10.31	9.91	13.11	19.11	20.50	14.56	14.89	17.45	8.02	7.28	7.74	12.35	8.50	10.19	5.92	3.94	12.86	17.44	15.28	10.30
6	4.30	24.24	21.61	7.18	7.79	5.82	8.92	11.03	$+\infty$	14.87	13.94	18.39	10.59	11.37	8.35	10.21	13.46	7.53	11.50	13.02	12.99	12.69	14.74	4.30	9.23	17.69	19.26	6.69	9.09
7	11.44	37.02	24.35	11.72	17.96	13.70	7.56	9.05	16.09	$+\infty$	11.17	8.30	24.52	25.79	20.80	21.67	24.22	14.79	10.57	6.07	11.03	5.87	4.51	11.44	6.76	12.64	21.90	19.67	11.13
8	9.66	36.71	14.63	6.77	12.45	14.60	9.88	8.75	14.59	10.64	$+\infty$	7.04	22.71	24.09	17.87	17.20	19.02	10.33	3.06	5.59	15.30	11.07	12.06	9.66	7.69	3.75	12.39	19.06	14.95
9	14.78	40.71	19.76	13.68	19.39	18.04	12.05	11.74	19.43	6.84	7.58	$+\infty$	27.86	29.13	24.00	24.11	25.96	17.24	9.97	6.54	16.53	11.59	10.23	14.78	9.86	7.91	18.10	23.07	16.63
10	13.78	24.27	24.73	15.87	11.65	15.63	18.53	20.64	10.32	24.48	22.61	28.00	$+\infty$	2.56	5.98	7.45	10.56	13.83	20.19	22.63	22.61	22.31	24.35	13.78	18.84	26.36	22.96	11.91	18.70
11	14.82	21.90	26.73	17.19	13.65	14.99	19.57	21.68	10.92	25.52	23.95	29.04	2.28	$+\infty$	8.26	9.73	12.84	15.83	21.52	23.67	22.40	23.35	25.39	14.82	19.87	27.70	24.96	11.25	18.39
12	11.09	29.06	19.54	11.38	6.45	13.43	15.26	16.57	7.75	21.13	17.72	23.93	6.10	8.30	$+\infty$	2.58	5.83	8.63	15.65	18.56	19.91	19.32	21.01	11.09	14.76	21.44	17.76	12.34	16.01
13	12.44	31.22	17.83	11.19	5.98	14.78	16.28	17.59	9.11	22.16	17.32	24.35	7.84	10.04	2.73	$+\infty$	3.52	8.23	15.24	19.58	21.26	20.34	22.03	12.44	15.79	21.04	16.40	14.78	17.36
14	14.97	34.25	16.96	13.17	7.76	18.08	18.28	19.60	12.40	24.16	18.76	25.80	10.81	12.81	5.98	3.53	$+\infty$	10.21	16.68	21.59	24.52	22.34	24.03	14.97	17.79	22.04	16.10	18.07	20.65
15	5.75	31.13	15.96	3.96	4.45	10.99	9.06	10.38	7.58	14.94	10.09	17.12	14.20	16.12	9.01	8.35	10.91	$+\infty$	8.01	12.37	15.30	13.12	14.81	5.75	8.57	13.84	13.59	14.00	12.42
16	6.87	33.91	15.37	3.97	9.82	11.81	8.36	8.16	11.79	10.28	3.32	10.03	19.91	21.30	15.08	14.41	16.40	7.54	$+\infty$	5.23	14.82	10.60	11.59	6.87	7.10	6.95	12.92	16.27	12.25
17	9.48	35.40	18.53	8.50	14.35	12.74	6.74	6.12	14.12	5.76	5.35	6.28	22.55	23.83	18.70	18.93	20.92	12.06	4.75	$+\infty$	11.69	7.47	7.32	9.48	4.55	7.31	16.09	17.76	11.79
18	9.96	29.73	27.42	12.39	18.63	8.19	7.80	10.77	14.04	10.52	15.04	16.52	22.28	22.04	20.22	21.61	24.76	15.33	14.23	11.23	$+\infty$	5.26	8.13	9.96	8.48	17.05	24.98	13.85	5.44
19	8.93	32.97	24.51	9.94	16.18	8.96	5.38	7.27	13.53	5.95	11.53	12.10	21.96	23.23	19.02	19.88	22.44	13.01	10.73	7.47	5.46	$+\infty$	3.57	8.93	4.98	13.54	22.06	15.95	5.79
20	11.34	36.62	25.14	11.62	17.85	12.61	7.41	8.94	15.98	4.63	12.16	11.23	24.41	25.69	20.69	21.56	24.12	14.69	11.36	7.13	8.98	3.74	$+\infty$	11.34	6.65	13.83	22.69	19.57	9.44
21	$+\infty$	28.10	19.06	3.01	9.40	6.76	5.17	7.29	5.67	11.12	9.77	14.64	14.10	15.37	11.16	12.26	14.96	5.53	7.29	9.28	10.73	9.30	11.00	$+\infty$	5.48	13.52	16.61	10.46	7.85
C_1	5.48	31.41	20.03	5.52	11.76	8.74	2.75	2.51	10.12	6.58	7.05	9.39	18.56	19.83	14.70	15.56	18.12	8.69	6.25	4.02	8.88	4.88	6.46	5.48	$+\infty$	9.14	17.58	13.76	7.82
C_2	13.40	40.45	12.12	10.51	15.07	18.31	12.31	11.57	18.32	12.35	3.81	7.57	26.30	27.83	21.12	20.45	21.65	14.07	6.80	7.80	17.71	13.49	13.96	13.40	10.12	$+\infty$	10.46	22.80	17.39
C_3	16.81	42.46	2.96	14.08	12.38	22.39	19.11	19.30	18.92	21.37	12.13	17.67	22.61	24.73	17.38	16.20	16.31	13.81	12.93	16.32	25.63	21.75	22.74	16.81	18.15	10.23	$+\infty$	25.34	23.00
C_4	9.62	17.96	27.16	12.63	13.34	7.36	13.25	15.58	7.81	19.41	19.02	22.93	11.04	10.80	12.50	15.01	18.27	13.61	16.40	17.56	13.93	16.21	19.28	9.62	13.77	22.68	24.81	$+\infty$	10.76
C_5	7.21	27.43	25.23	10.20	14.79	3.82	5.61	9.87	9.96	11.16	14.89	16.89	18.40	18.45	16.15	17.53	20.79	12.73	12.62	11.59	4.85	6.27	9.71	7.21	7.97	16.97	22.78	10.52	$+\infty$

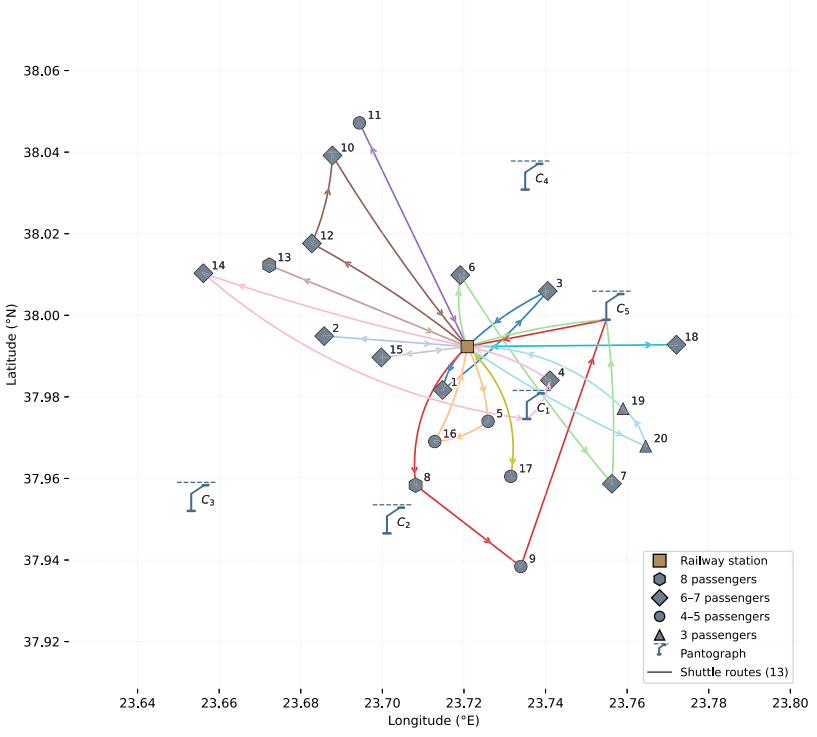

Fig. C.11. Travel route paths of the $\epsilon = 13$ electric shuttles (Deterministic Approach).

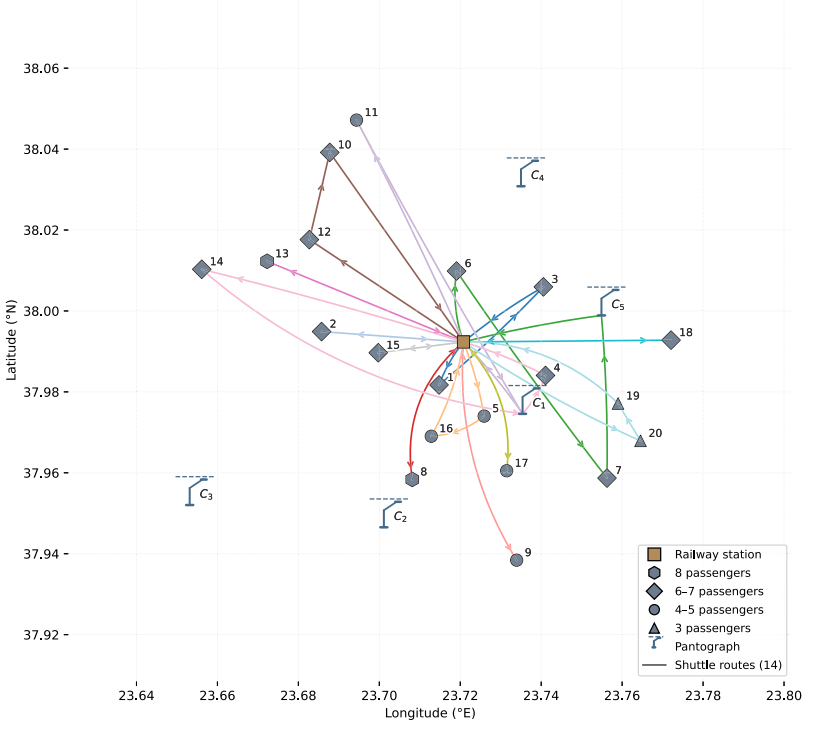

Fig. C.12. Travel route paths of the $\epsilon = 14$ electric shuttles (Deterministic Approach).

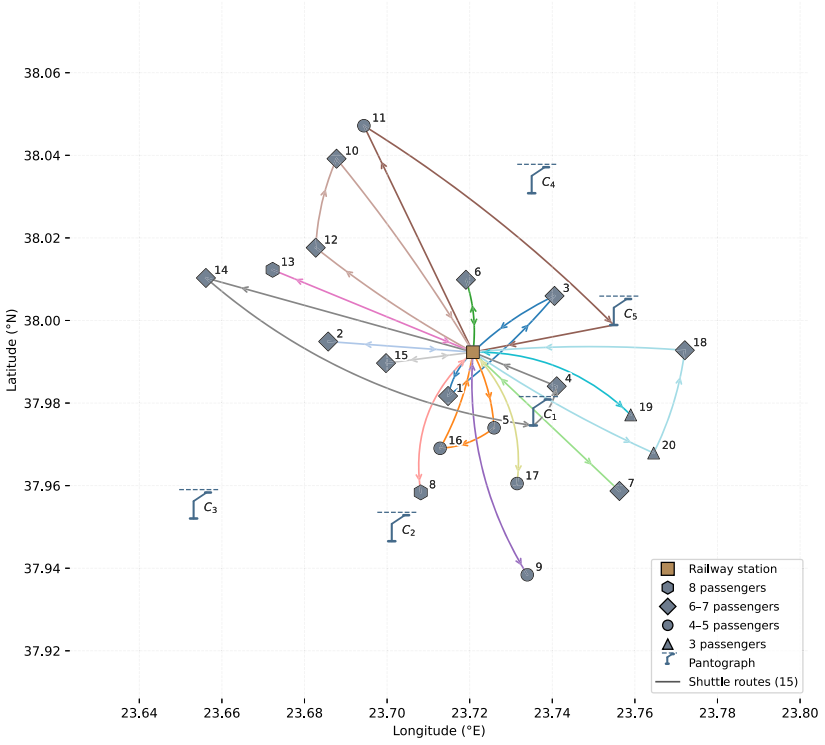

Fig. C.13. Travel route paths of the $\epsilon = 15$ electric shuttles (Deterministic Approach).

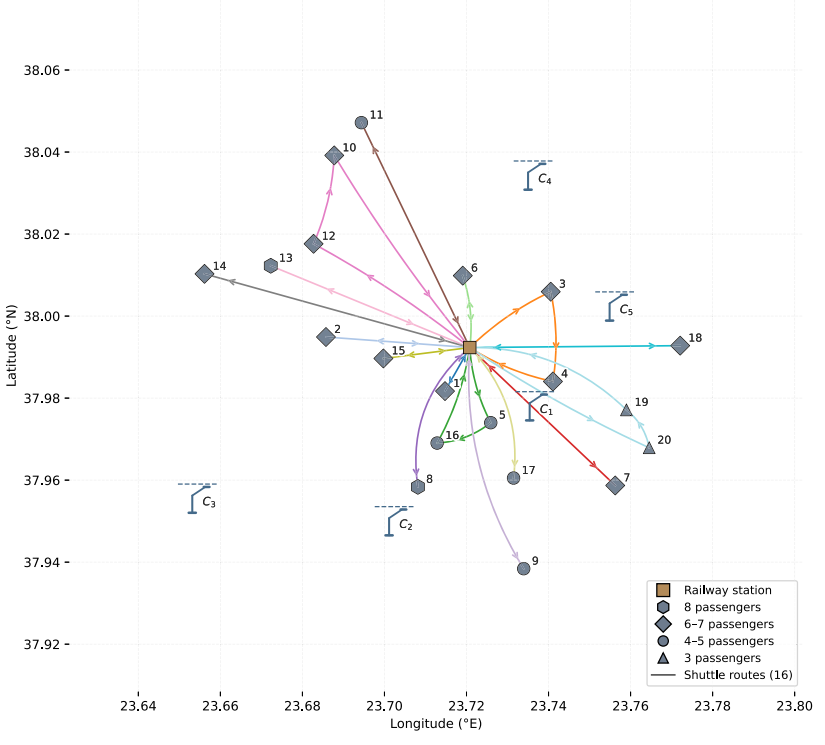

Fig. C.14. Travel route paths of the $\epsilon = 16$ electric shuttles (Deterministic Approach).

References

Abel, G., 2024. VDI / YUTONG. Technical Report. Sydney Business Scool. https://business.sydney.edu.au/_data/assets/pdf_file/0010/514576/Greg-Abel_without-videos.pdf.

Ahani, P., Arantes, A., Melo, S., 2023. An optimization model for structuring a car-sharing fleet considering traffic congestion intensity. J. Adv. Transp. 2023 (1), 9283130.

Aidam, G. S.K., Opoku, R., Adjei, E.A., Davis, F., Oppong, D.K., Adu-Poku, A., Agyare, W.G., Narh, A., Aidam, S.G., 2025. Electrified transportation for sustainable mobility in developing countries–a review of challenges and opportunities. J. Ghana Inst. Eng. 25 (1), 34–44.

AlHadidi, T., Rakha, H.A., 2019. Modeling bus passenger boarding/alighting times: a stochastic approach. Transp. Res. Interdiscip. Perspect. 2, 100027.

Alonso-González, M.J., van Oort, N., Cats, O., Hoogendoorn, S., 2017. Urban demand responsive transport in the mobility as a service ecosystem: its role and potential market share. In: International Conference Series on Competition and Ownership in Land Passenger Transport (Thredbo 15), Stockholm, Sweden.

Badia, H., Jenelius, E., 2021. Design and operation of feeder systems in the era of automated and electric buses. Transp. Res. A Policy Pract. 152, 146–172. https://doi.org/10.1016/j.tra.2021.07.015

Boewing, F., Schiffer, M., Salazar, M., Pavone, M., 2020. A vehicle coordination and charge scheduling algorithm for electric autonomous mobility-on-demand systems. In: 2020 American Control Conference (ACC). IEEE, pp. 248–255.

Cabify, 2025. Ride safely and at the best price. Official riders page. Accessed 2025-09-28. https://cabify.com/en/riders.

Ceder, A., 2016. Public Transit Planning and Operation: Modeling, Practice and Behavior. CRC press.

Chen, T.D., Kockelman, K.M., 2016. Management of a shared autonomous electric vehicle fleet: implications of pricing schemes. Transp. Res. Rec. 2572 (1), 37–46. https://doi.org/10.3141/2572-05

Chen, T.D., Kockelman, K.M., Hanna, J.P., 2016. Operations of a shared, autonomous, electric vehicle fleet: implications of vehicle & charging infrastructure decisions. Transp. Res. A Policy Pract. 94, 243–254. https://doi.org/10.1016/j.tra.2016.08.020

Dang, L., von Arx, W., Frölicher, J., 2021. The impact of on-demand collective transport services on sustainability: a comparison of various service options in a rural and an urban area of switzerland. Sustainability 13 (6), 3091.

Dimitriadou, A., Gkiotsalitis, K., 2025. Multi-objective synchronization of public transport and shared modes: model and application. Transp. Res. Interdiscip. Perspect. 33, 101570.

Doubleday, K., Meintz, A., Markel, T., 2016. An opportunistic wireless charging system design for an on-demand shuttle service. In: 2016 IEEE Transportation Electrification Conference and Expo (ITEC), pp. 1–6. https://doi.org/10.1109/ITEC.2016.7520265

El Faouzi, N., Maurin, M., 2007. Reliability of travel time under log-normal distribution: methodological issues and path travel time confidence derivation. In: Transportation Research Board 86Th Annual Meeting (CD-ROM). Transportation Research Record, Washington, DC.

Elmenshawy, M., Massoud, A., 2022. Medium-voltage DC-DC converter topologies for electric bus fast charging stations: state-of-the-art review. Energies 15, 5487. https://doi.org/10.3390/en15155487

Estandia, A., Schiffer, M., Rossi, F., Luke, J., Kara, E.C., Rajagopal, R., Pavone, M., 2021. On the interaction between autonomous mobility on demand systems and power distribution networks—an optimal power flow approach. IEEE Trans. Control Netw. Syst. 8 (3), 1163–1176.

Esteban, J., Grahn, R., Powell, B., Young, S.E., 2025. Community public mobility using on-demand, low-speed electric vehicles: a case study in downtown st. louis, missouri. Transp. Res. Rec. 2679 (2), 390–402.

European Environment Agency, 2024. Air pollution: transport's contribution in the EU. Transport largest NOx emitter in EU-27; background context on air pollution. Accessed 2025-09-28. https://www.eea.europa.eu/en/analysis/publications/sustainability-of-europes-mobility-systems/air-pollution.

Fang, Y., 2025. Electric Vehicle Demand-Responsive Transport with Transit Integration. Doctoral thesis. University of Luxembourg. Esch-sur-Alzette, Luxembourg. https://hdl.handle.net/10993/64657.

Fang, Y., Ma, T.-Y., 2023. Demand responsive feeder bus service using electric vehicles with timetabled transit coordination. Springer, Germany. Lecture Notes in Intelligent Transportation and Infrastructure (LNITI), pp. 91–103. https://doi.org/10.1007/978-3-031-23721-8_7

Gao, J., Li, S., 2024. Charging autonomous electric vehicle fleet for mobility-on-demand services: plug in or swap out? Transp. Res. C Emerg. Technol. 158, 104457. https://doi.org/10.1016/j.trc.2023.104457

Gkiotsalitis, K., 2023. Public Transport Optimization. Springer Nature.

Gkiotsalitis, K., Cats, O., Liu, T., 2023. A review of public transport transfer synchronisation at the real-time control phase. Transp. Rev. 43 (1), 88–107.

Gkiotsalitis, K., Schmidt, M., van der Hurk, E., 2022. Subline frequency setting for autonomous minibusses under demand uncertainty. Transp. Res. C Emerg. Technol. 135, 103492.

Greenwheels, 2026. Greenwheels and NS partnership for shared mobility integration. https://www.greenwheels.com. Accessed: 2026-05-08.

Harris, I., Wang, Y., Wang, H., 2015. Ict in multimodal transport and technological trends: unleashing potential for the future. Int. J. Prod. Econ. 159, 88–103.

HelloRide Singapore, 2026. Helloride shared bicycle services in singapore. https://www.helloride.com. Accessed: 2026-05-08.

Hsueh, G., Czerwinski, D., Poliziani, C., Becker, T., Hughes, A., Chen, P., Benn, M., 2021. Using BEAM Software to Simulate the Introduction of On-Demand, Automated, and Electric Shuttles for Last Mile Connectivity in Santa Clara County. Final Report 20–47. Mineta Transportation Institute, San Jose State University. https://doi.org/10.31979/mti.2021.1822

International Energy Agency, 2023. CO2 Emissions in 2022: Growth in emissions lower than feared. Technical Report. IEA. Global CO2 = 36.8 Gt in 2022. Accessed 2025-09-28. https://iea.blob.core.windows.net/assets/3c8fa115-35c4-4474-b237-1b00424c8844/CO2Emissionsin2022.pdf.

ITS International, 2022. Shotl delivers lisbon DRT system. ITS Int. Mentions Xbus app for requests. Accessed 2025-09-28. https://www.itsinternational.com/its6/its8/news/shotl-delivers-lisbon-drt-system.

Jara-Díaz, S., Tirachini, A., 2013. Urban bus transport: open all doors for boarding. J. Transp. Econ. Policy 47 (1), 91–106.

Jäger, B., Agua, F. M.M., Lienkamp, M., 2017. Agent-based simulation of a shared, autonomous and electric on-demand mobility solution. In: 2017 IEEE 20th International Conference on Intelligent Transportation Systems (ITSC), pp. 250–255. https://doi.org/10.1109/ITSC.2017.8317947

Kaddoura, I., Leich, G., Nagel, K., 2020. The impact of pricing and service area design on the modal shift towards demand responsive transit. Procedia Comput. Sci. 170, 807–812.

Kim, S., Pasupathy, R., Henderson, S.G., 2015. A guide to sample average approximation. Handb. Simul. Optim. 216, 207–243.

Land Transport Authority Singapore, 2019. Land transport master plan 2040. https://www.lta.gov.sg/content/ltagov/en/who_we_are/our_work/land_transport_master_plan_2040.html. Accessed: 2026-05-08.

Li, X., Huang, J., Guan, Y., Li, Y., Yuan, Y., 2022. Electric demand-responsive transit routing with opportunity charging strategy. Transp. Res. D Transp. Environ. 110, 103427. https://doi.org/10.1016/j.trd.2022.103427

Liang, Y., Ding, Z., Ding, T., Lee, W.-J., 2021. Mobility-aware charging scheduling for shared on-demand electric vehicle fleet using deep reinforcement learning. IEEE Trans. Smart Grid 12 (2), 1380–1393. https://doi.org/10.1109/TSG.2020.3025082

Liu, T., Cats, O., Gkiotsalitis, K., 2021. A review of public transport transfer coordination at the tactical planning phase. Transp. Res. C Emerg. Technol. 133, 103450.

Liyanage, S., Dia, H., 2025. On-demand technologies for public transport: insights from a Melbourne survey. IEEE Open J. Intell. Transp. Syst. 6, 653–672. https://doi.org/10.1109/OJITS.2025.3567075

Lott, J.S., Young, S.E., 2023. Automated electric vehicle fleet operations for on-demand service: challenges and opportunities. In: International Conference on Transportation and Development 2023, pp. 552–564.

Makarova, I., Serikkaliyeva, A., Gubacheva, L., Mukhametdinov, E., Buyvol, P., Barinov, A., Shepelev, V., Mavlyautdinova, G., 2023. The role of multimodal transportation in ensuring sustainable territorial development: review of risks and prospects. Sustainability 15 (7), 6309.

Mazloumi, E., Currie, G., Rose, G., 2010. Using GPS data to gain insight into public transport travel time variability. J. Transp. Eng. 136 (7), 623–631.

McCoy, K., Andrew, J., Glynn, R., Lyons, W., et al., 2018. Integrating shared mobility into multimodal transportation planning: improving regional performance to meet public goals. Technical Report. Federal Highway Administration, United States.

Melo, S., Gomes, R., Abbasi, R., Arantes, A., 2024. Demand-responsive transport for urban mobility: integrating mobile data analytics to enhance public transportation systems. Sustainability 16 (11), 4367.
(NS), N.S., 2026. Ov-fiets: Bicycle sharing service integrated with dutch rail transport. https://www.ns.nl/deur-tot-deur/ov-fiets. Accessed: 2026-05-08.
Paparella, F., Chauhan, K., Koenders, L., Hofman, T., Salazar, M., 2025. Ride-pooling electric autonomous mobility-on-demand: joint optimization of operations and fleet and infrastructure design. Control Eng. Pract. 154, 106169.
Paparella, F., Hofman, T., Salazar, M., 2024. Electric autonomous mobility-on-demand: jointly optimal vehicle design and fleet operation. IEEE Trans. Intell. Transp. Syst. 25 (11), 17054–17065. https://doi.org/10.1109/TITS.2024.3428569
Rahman, M.M., Wirasinghe, S.C., Kattan, L., 2018. Analysis of bus travel time distributions for varying horizons and real-time applications. Transp. Res. C Emerg. Technol. 86, 453–466.
Rossi, F., Iglesias, R., Alizadeh, M., Pavone, M., 2019. On the interaction between autonomous mobility-on-demand systems and the power network: models and coordination algorithms. IEEE Trans. Control Netw. Syst. 7 (1), 384–397.
Salazar, M., Rossi, F., Schiffer, M., Onder, C.H., Pavone, M., 2018. On the interaction between autonomous mobility-on-demand and public transportation systems. In: 2018 21St International Conference on Intelligent Transportation Systems (ITSC), pp. 2262–2269. https://doi.org/10.1109/ITSC.2018.8569381
SBS Transit, 2026. Integration of anywheel bicycle sharing with SBS transit services. https://www.sbstransit.com.sg. Accessed: 2026-05-08.
Shams Ashkezari, L., Jafari Kaleybar, H., Brenna, M., Zaninelli, D., 2022. E-bus opportunity charging system supplied by tramway line: a real case study. pp. 1–6. https://doi.org/10.1109/EEEIC/ICPSEurope54979.2022.9854598
Shams Ashkezari, L., Kaleybar, H.J., Brenna, M., 2024. Electric bus charging infrastructures: technologies, standards, and configurations. IEEE Access 12, 80505–80528. https://doi.org/10.1109/ACCESS.2024.3410880
Sheppard, C. J.R., Bauer, G.S., Gerke, B.F., Greenblatt, J.B., Jenn, A.T., Gopal, A.R., 2019. Joint optimization scheme for the planning and operations of shared autonomous electric vehicle fleets serving mobility on demand. Transp. Res. Rec. 2673 (6), 579–597.
Shotl, 2022. Shotl's first inner-city service in lisbon. Users request via Xbus (Carris); 61 virtual stops, weekday service. Accessed 2025-09-28. https://shotl.com/news/shotls-first-inner-city-service-in-lisbon.
State of Berlin, 2022. Berlkönig. City information page. Accessed 2025-09-28. https://www.berlin.de/en/getting-around/ridesharing/6008199-6052076-berlkoenig.en.html.
Steiner, K., Irnich, S., 2020. Strategic planning for integrated mobility-on-demand and urban public bus networks. Transp. Sci. 54 (6), 1616–1639.
Sun, X., Zu, Y., 2025. Research on fleet size of demand response shuttle bus based on minimum cost method. Appl. Sci. 15 (10), 5350.
Tan, W., Sun, Y., Ding, Z., Lee, W.-J., 2022. Fleet management and charging scheduling for shared mobility-on-demand system: a systematic review. IEEE Open Access J. Power Energy 9, 425–436.
Tucker, N., Turan, B., Alizadeh, M., 2019. Online charge scheduling for electric vehicles in autonomous mobility on demand fleets. In: 2019 IEEE Intelligent Transportation Systems Conference (ITSC), pp. 226–231. https://doi.org/10.1109/ITSC.2019.8917101
Uber Technologies, I., 2025. Request rides 24/7. Official ride request page. Accessed 2025-09-28. https://www.uber.com/us/en/ride/.
ViaVan, 2018. Viavan and BVG launch BerlKönig in berlin. Official launch release. Accessed 2025-09-28. https://ridewithvia.com/news/viavan-and-bvg-launch-berlkonig-in-berlin.
Wang, N., Guo, J., 2022. Multi-task dispatch of shared autonomous electric vehicles for mobility-on-demand services–combination of deep reinforcement learning and combinatorial optimization method. Heliyon 8 (11), e11319.
Wang, Y., Dong, W., Zhang, L., Chin, D., Papageorgiou, M., Rose, G., Young, W., 2012. Speed modeling and travel time estimation based on truncated normal and lognormal distributions. Transp. Res. Rec. 2315 (1), 66–72.
Xiong, J., Chen, B., Li, X., He, Z., Chen, Y., 2020. Demand responsive service-based optimization on flexible routes and departure time of community shuttles. Sustainability 12 (3), 897.
Xue, Y., Zhong, M., Xue, L., Zhang, B., Tu, H., Tan, C., Kong, Q., Guan, H., 2022. Simulation analysis of bus passenger boarding and alighting behavior based on cellular automata. Sustainability 14 (4), 2429.
Zeelo, 2025. Zeelo | group transportation services. Company overview. Accessed 2025-09-28. https://zeelo.co/.
Zghidi, I., Hnich, B., Rebaï, A., 2018. Modeling uncertainties with chance constraints. Constraints 23, 196–209.
Zhang, X., Wu, Y., 2023. Analysis of public transit operation efficiency based on multi-source data: a case study in brisbane, australia. Res. Transp. Bus. Manag. 46, 100859.